August, 2016

EXTENDING LORENTZ' NETWORK MODEL FOR THE DUTCH WADDEN SEA

A MATTER OF TIME

MSc Thesis

Author:
K.R.G. Reef

Supervisors:
Prof. dr. S.J.M.H. Hulscher
Dr. ir. P.C. Roos
Dr. G. Lipari

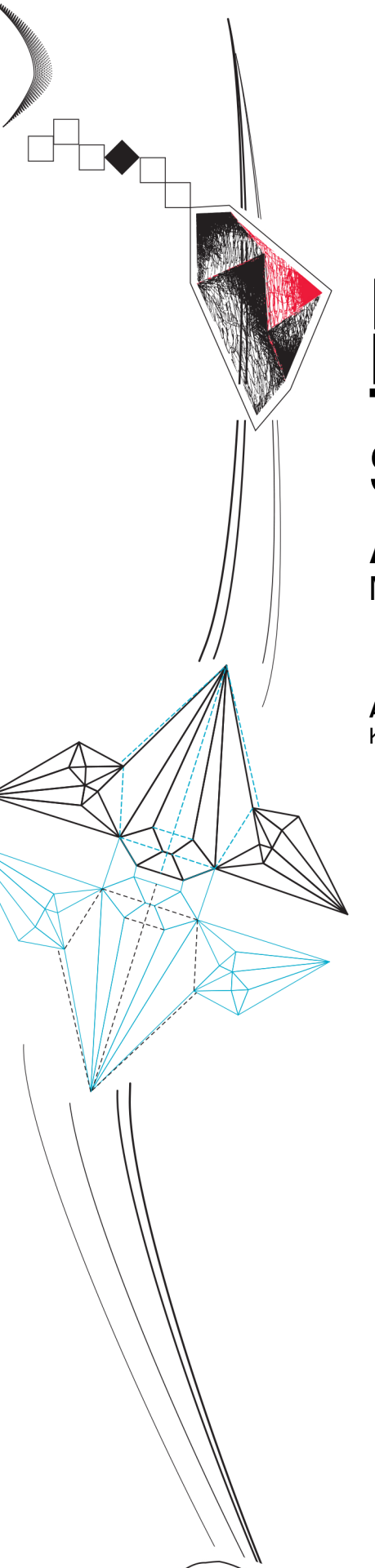

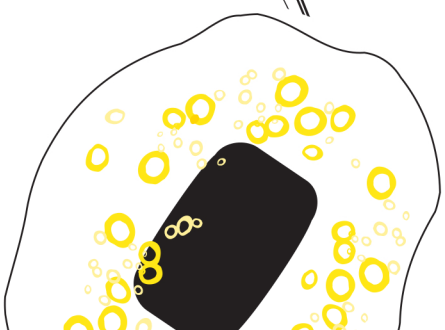

Waterbeweging Watermotion

UNIVERSITY OF TWENTE.

Abstract

Between 1918 and 1926 the State Committee on the Zuiderzee investigated the hydrodynamic effects of damming the Dutch Zuiderzee ahead of the prospected construction of the so-called Afsluitdijk. The State Committee, chaired by physicist and Nobel laureate H.A. Lorentz, developed a network model based on the governing equations of fluid flow, rather than on empirical relationships in order to assess the effects of the closure dam on the water motions in the Wadden Sea.

Strongly simplified network models were developed to simulate tidal water motions and an equilibrium response to a steady wind forcing, thereby ignoring the transient phase towards this equilibrium. This study aims at developing a non-stationary network model to study the transient behaviour of storm-surges based on the simplification Lorentz used.

First the simulations from the State Committee have been resimulated. The resulting water level increase of the rebuilt storm-surge model is shown in Figure 1. The results show a good quantitative and qualitative agreement with the values found by the State Committee.

Next a non-stationary model – allowing for a time dependent wind stress – has been developed and used to: (1) mimic the equilibrium model by including a ramp up and ramp down period, (2) model the 22/23 December 1894 storm on which the equilibrium model was based, (3) simulate the 5 December 2013 'Sinterklaas' storm for which recent water level and wind stress measurements are available.

The results show that: (1) the non-stationary model is able to mimic the stationary model when the same forcing is applied, (2) the water levels during the 22/23 December 1894 peak after the wind stress has peaked, (3) the 5 December 2013 storm is simulated well qualitatively and reasonably quantitatively (as can be seen in Figure 2).

The results indicate that a simple network model can be used to simulate storm-surges in the Wadden Sea. Despite the simplifications the model performs relatively well since water levels are simulated reasonably accurate. Using this model the temporal behaviour of storm-surges has been studied such as the peak timing and the rise and fall of the water level

Preface

"There is no future without a past, because what is to be cannot be imagined except as a form of repetition." – Siri Hustvedt

This thesis marks the end of my graduation project and the end of my study Water Engineering & Management at the University of Twente. This report covers the use of a simplified model that is used to simulate storm surges in the Wadden Sea. It is inspired by the work that the State Committee on the Zuiderzee — chaired by H.A. Lorentz — did in advance of the construction of the Afsluitdijk and this thesis would not have been possible without their work almost 100 years ago.

During the last six months I had the pleasure to work on a very enjoyable combination of physics, mathematics, and model building to study storm surges in the Wadden Sea using a strongly simplified model. Although much has been done in the Netherlands in the last century to prevent flood damage from storm surges they continue to pose a severe threat to lower areas. Nowadays complex hydrodynamical models are used to simulate water motions in the seas surrounding the Netherlands, but this study revisits the simple models that were used to assess the hydrodynamic impact of the Afsluitdijk.

This work would not have been possible without the excellent supervisors that provided support during this project. Your diverse backgrounds helped to put things into a wider perspective. I want to thank Pieter for his support, thorough feedback, and his mathematical insights which contributed to the basis of this project. I want to thank Giordano for his knowledge on storms, storm surges, and his thorough feedback especially on this report. I want to thank Suzanne for her questions, useful suggestions and the opportunity to graduate at the Water Engineering & Management group. Finally I want to thank Huib de Swart for his knowledge on the work of the State Committee and the insight that he provided.

I also need to thank my fellow graduate students at Z-134 with whom I had an excellent time during my graduation project. I want to thank them for the atmosphere that was a good mix of productivity and having fun. I want to thank them for the good coffee that we made every day. And most importantly I want to thank them for the good discussion that we had that helped all of us in getting better work done.

Koen Reef

Contents

1 Introduction

Storm surges have always threatened low lying areas as the Netherlands. At the end of the 19th century a plan was drafted to build a closure dam to disconnect a large bay — the Zuiderzee, now called lake IJssel — from the Wadden Sea to better protect the lands around the Zuiderzee. Before the dam was built proponents argued that it would improve the safety of the lands surrounding the Zuiderzee and it would enable vast land reclamations within the Zuiderzee. Opponents argued that a closure dam would lead to higher water levels in the Wadden Sea and it would have a devastating impact on fishing communities surrounding the Zuiderzee. To assess the hydrodynamic impact of a closure dam the State Committee (SC) on the Zuiderzee was established and they finished their investigation in 1926 resulting in an extensive report (State Committee on the Zuiderzee, 1926).

In this study we revisit the strongly simplified simulations that the SC used to assess the hydrodynamic impact of a closure dam and we develop a new storm surge model that uses most of the simplifications that the SC used whilst incorporating a time-dependent wind forcing.

In this chapter background information is given for: storm surges in the Dutch Wadden Sea (section 1.1), the State Committee and their research (section 1.2), and recent developments in network models (section 1.3). This is followed by the research aim (section 1.4), research questions (section 1.5), outline of the methodology (section 1.6), and the report outline (section 1.7).

1.1. Storm surges in the Dutch Wadden Sea

A storm is a meteorological phenomenon that is associated with low atmospheric pressure and strong winds with high wind speeds. Since there is an inverse relationship between sea-level and atmospheric pressure (Pugh, 1987), low atmospheric pressure associated with storms causes higher water levels at coasts. The effect of the wind on the water body is twofold, first, the wind stress acting on the water induces a flow of water in the direction of the wind and consequently higher water levels at the coast. Secondly the wind stress lead to the occurrence of wind waves on the water body causing run-up on flood defences, threatening their integrity. During a storm the tidal water motions continue, when the storm-induced water level or storm surge coincides with high tidal water levels (e.g. during spring tide) serious coastal flooding can occur, as happened in the southern part of the Netherlands in 1953 (e.g. Gerritsen, 2005).

Figure 1.1: The Dutch Wadden Sea seen from above with the Afsluitdijk just above centre separating lake IJssel from the Wadden Sea (United States Geological Survey, 2016).

The Dutch Wadden Sea (a satellite image is shown in Figure 1.1) is a shallow sea that lies in the northern part of the Netherlands in between the North Sea and the Dutch mainland. It is part of the larger Wadden Sea that stretches from the Netherlands through Germany to Denmark. The Dutch Wadden Sea consists of deep channels that connect to the North Sea through tidal inlets and of tidal flats in between the channels. Since it is connected to the North Sea through inlets, it experiences tides and storm surges that enter from the North Sea. This also held for the Zuiderzee that was connected to the North Sea through the Wadden Sea. According to Pugh (1987) storms have the greatest effect where they act on shallow seas, of which the Wadden Sea is an example.

1.2. The State Committee and Lorentz' models

The State Committee, chaired by physicist and Nobel laureate H.A. Lorentz, developed a network model based on the governing equations of fluid flow, rather than on empirical relationships, in order to assess the effects of the closure dam on the water motions in the Wadden Sea, due to both tide and storms. It was Lorentz' conviction that a thorough theoretical investigation was necessary for such a large-scale coastal engineering work (e.g. Mazure, 1963 and Kox, 2007). The approach developed by Lorentz uses a strongly simplified process-based hydrodynamic model to quantify the effects that a closure dam would have on the water motions. This theoretical approach provided accurate predictions and proved the usefulness of a process-based approach.

Tides and storm surges were simulated by the SC to study the effects of a closure dam. The tide and storm surge simulations were based on strong simplifications. Only the flow in channels was considered (one dimensional model), nonlinearities were neglected in the tidal simulations, and a novel and elegant parametrization — known as Lorentz' linearisation (Lorentz, 1922) — was used to represent bottom friction. The simplifications underlying the storm surge simulation were even more significant, since only a stationary situation was considered and the transient stage towards equilibrium was ignored. Yet the model retains the most important processes governing the water motion. A non-stationary storm surge model was developed for a strongly simplified case to quantify the error that was present in the stationary storm surge simulation.

1.3. Network models

Since the investigations by the SC the field of coastal physics has evolved with new models and applications. Other network based models have been used to simulate the tide and wind influence in the Oosterschelde (Stroband and Wijngaarde, 1977). The interaction of surge and tide in the North Sea and River Thames has been studied by

Prandle and Wolf (1978), concluding that bottom friction is the dominant interaction mechanism. More recently, Bakker and de Vriend (1995) used a network based model (extending Lorentz's approach) to determine resonance and morphological stability in the Wadden Sea.

Hill and Souza also presented a tidal network model aiming at providing a rapid assessment of the tidal response. Their approach was developed for a single channel (Souza and Hill, 2006) and for a network (Hill and Souza, 2006). The model proved to be effective in simulating tides in the Menai Strait and a fjordic network off Western Canada. It allows for a rapid assessment of the tide without the need of large data sets. A limitation is that nonlinear terms are excluded limiting the applicability in e.g. shallower basins.

Even more recently, Alebregtse et al. (2013) presented a network model based on the linearised, one-dimensional shallow water equations to study the resonance characteristics of tides in branching channels. Alebregtse and de Swart (2014) extended this by using a nonlinear model in which the water motion is described by the one-dimensional, nonlinear, cross-sectionally averaged shallow water equations. In another study Alebregtse and de Swart (2016) studied the effect of river discharge and geometry on tides and net water transport in an estuarine network using an idealized schematisation of the Yangtze Estuary, China. They found that an increase in river discharge would lead to an increase of the semi-diurnal tide.

Besides the idealized process-based model that focusses on the dominant processes (such as the model by Lorentz), more complete models exist that include as many processes as possible. An example is the Dutch Continental Shelf Model that is used in the Netherlands for sea water level predictions (e.g. Zijl et al., 2013). It solves the nonlinear shallow water equations on a grid and is based on the WAQUA solver (Stelling, 1983).

1.4. Research aim

Tidal network models have been improved since Lorentz first worked on them, tide-surge interactions have been studied and nonlinear dynamics have been incorporated. Meanwhile complex storm models have also been developed, but network-based storm surge models have hardly advanced. Therefore, this study aims at developing a non-stationary storm surge network model that uses the same domain and is based on the same equations as Lorentz' storm surge model whilst it is forced by a non-stationary wind-field, to study the transient behaviour of storm surges.

1.5. Research questions

In order to achieve the objective, two main research questions are posed:

1. How can a non-stationary model be developed based on Lorentz' approach as to simulate non-stationary storm surges forced by a time-dependent wind field?
2. In which aspects do the results of the non-stationary storm surge simulations differ from the results of the stationary storm surge simulation?
   (a) How do the results of the non-stationary storm surge simulations relate to the results of the stationary storm surge simulation?
   (b) Which insights gained from the non-stationary results cannot be found in the stationary results?
   (c) What is the accuracy of the model if it is applied to a recent storm?

1.6. Outline of the methodology

In this study a non-stationary model is developed based on Lorentz' approach and used to investigate storm surges. The model is based on the linearised shallow water equations and solved in the frequency domain. To this end a Fourier transformation is applied to the input (time dependent wind stress) and the output (water level and flow velocity). By linearity a superposition of the solution for each individual frequency gives the solution to the original problem in the time domain.

Three wind events are modelled:

- a wind event to mimic the stationary storm surge simulation,
- the storm of 22/23 December 1894 to find the temporal relationship between the highest wind stress and highest water levels,
- the storm of 5 December 2013 to assess the qualitative and quantitative model performance.

By comparing the results of the first event with the results of the stationary storm surge simulation of the SC a comparison can be made between the two models to find similarities and differences. The second event is compared to measurements of the 1894 storm to assess the timing of peak water levels. The third event is compared to recent water level measurements to assess the model accuracy.

1.7. Report outline

This report is structured as follows:

Chapter 2 describes the model and the methods used in this study. This includes reproducing the original results by the SC, new model runs to study the temporal behaviour of storm surges, and a sensitivity analysis. By describing how the non-stationary storm surge model is obtained, the first research question is answered.

Chapter 3 describes the results that have been found using the model developed in this study. The reproduced SC results are compared with those obtained by the SC. Both the results for the new simulations and the results of the sensitivity analysis are presented in this chapter. Thereby answering research question two.

Chapter 4 discusses the limitations of the approach and the results are interpreted. This includes the reproduced SC results, the new solution, its sensitivity analysis and the role of nonlinearities.

Chapter 5 presents the answers to the research questions and the conclusions.

2 Model and Methods

2.1. Hydrodynamic model

2.1.1 Domain

The Wadden Sea — consisting of deep channels and shallow tidal flats as shown in Figure 1.1 — was schematized into multiple networks of interconnected channels by the SC . The tidal network (shown in Figure 2.1) covers the Dutch Wadden Sea from the Marsdiep inlet near Den Helder to the Amelander inlet between Terschelling and Ameland and covers the entire Zuiderzee.

The storm network (shown in Figure 2.2) covers the Dutch Wadden Sea from the Marsdiep inlet, near Den Helder, to the Frisian inlet between Ameland and Schiermonnikoog and ends at the entrance to the Zuiderzee. To mimic the effect that the Zuiderzee would have had on the Dutch Wadden Sea, a constant outflow was imposed at the entrance of the Zuiderzee.

The main differences between both networks are the amount of channels used to represent the Wadden Sea — i.e. more channels are used in the tidal network than in the storm network — and the channel dimensions since the channels in the storm network are wider and thus have a larger cross-sectional area. The larger channels in the storm network accommodate the larger discharges that occur during storm conditions where more water flows over the tidal flats than during tidal conditions where little flows over the tidal flats.

These two networks have been used in this study, as well as three variations of these networks. The first is a variation of the tidal network, besides the version shown in Figure 2.1 a version without the Zuiderzee has been used to represent the Wadden Sea with a closure dam in place. The second is a variation of the storm network where the Zuiderzee has been added to the network at its ending near the entrance of the Zuiderzee. The channels used to represent the Zuiderzee in this network are the same as in the tidal network. The third is a variation of the storm network where also the entrance to the Zuiderzee is excluded as if the Afsluitdijk would be in place.

The characteristics of the channels in the tidal network are provided in Table 6 of the SC report (1926, §45) or Table A.2 in Appendix A. These channel characteristics have been used in this study with the exception of the velocity scale of channel 6a and the geometry of channel 20b. The velocity scale of channel 6a was inconsistent with data regarding the maximum discharge through the channel, i.e. a velocity scale

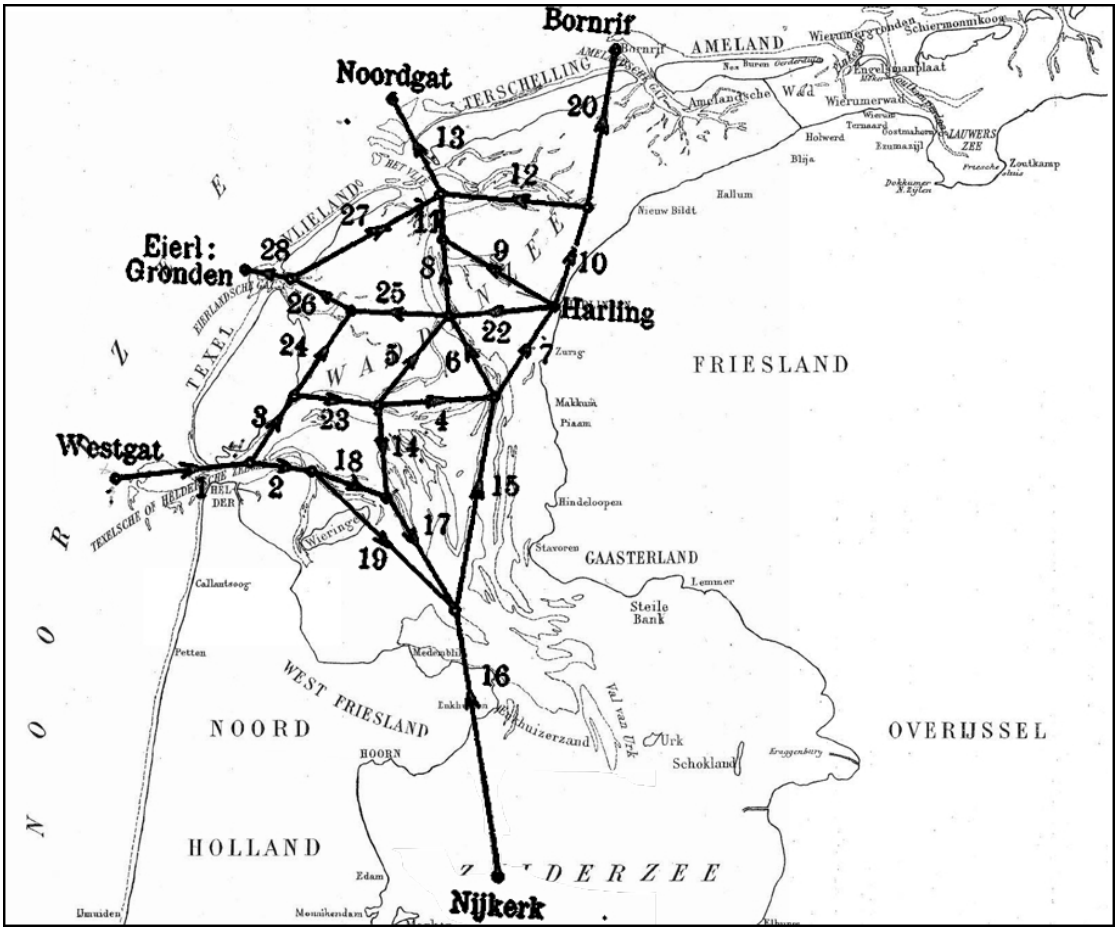

Figure 2.1: The channels representing the Dutch Wadden Sea prior to the construction of the Afsluitdijk. Showing the tidal network as used by the SC (1926, §45), with numbered channels.

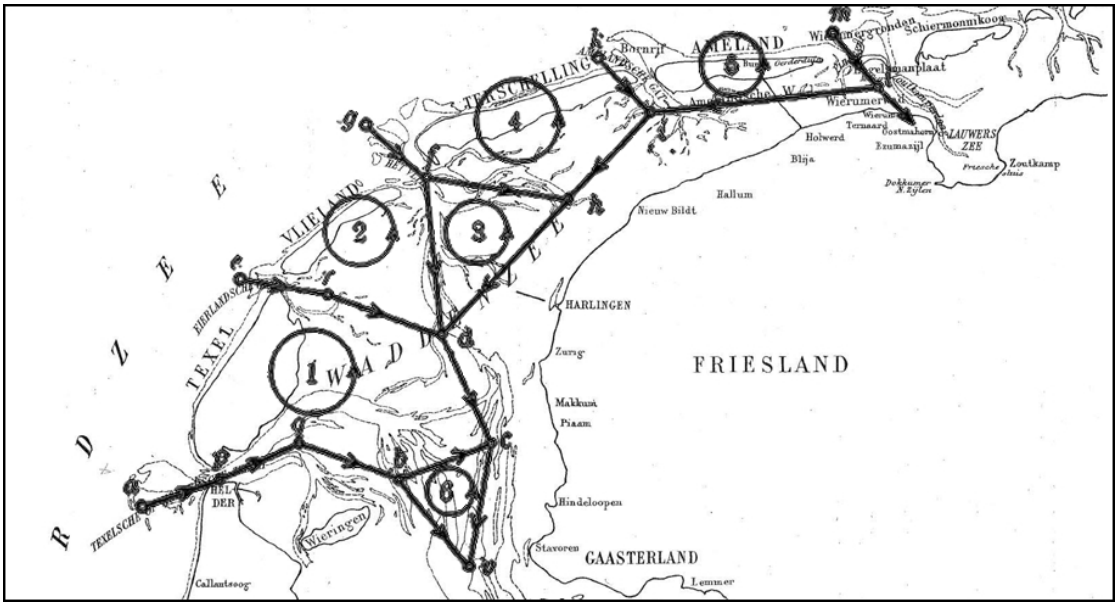

Figure 2.2: The channels representing the Dutch Wadden Sea prior to the construction of the Afsluitdijk. Showing the storm network as used by the SC (1926, §89), with lettered nodes.

of 26.5 cm s^{-1} was given whereas 90 cm s^{-1} would result in the maximum discharge specified. Thus a velocity scale of 90 cm^{-1} has been used for channel 6a.

For channel 20b the width and height of the channel was not given. The results obtained using an average channel width derived from the surface area of the water body divided by its length, yielded results differing considerably from those found by the SC with their model.

The region represented by channel 20b is similar to the adjacent region of channel 20a, as is shown in Figure 29 of the SC report and from aerial photography. Therefore, it is assumed that channel 20b contains similar sub-channels as channel 20a, with identical channel characteristics.

The velocity scale for channel 20b has been determined by dividing the maximum discharge by the cross-sectional area. Calculations with the original and revised channel configurations showed that the model with the adjusted input performs closely to the SC model, thus it is likely that the wrong values were typos in the SC report.

The characteristics of the channels in the storm network are provided in Table 19 of the SC report (1926, §89) and Table A.1 in Appendix 1. These channel characteristics have been used for the storm network in this study without changes.

2.1.2 Hydrodynamics

For every channel c in the network the hydrodynamics are governed by the cross-sectionally averaged one-dimensional linearised shallow-water equations:

$$\frac{\partial \zeta}{\partial t} + h\frac{\partial u}{\partial x} = 0, \tag{2.1}$$

$$\frac{\partial u}{\partial t} + \frac{r}{h}u + g\frac{\partial \zeta}{\partial x} = \frac{\tau_w}{\rho h}\cos\phi, \tag{2.2}$$

with ζ the water level, h the mean water depth, u the cross sectionally averaged flow velocity along the channel (x-direction), r the linear friction coefficient (see next sub-section), g = 9.81 m s^{-2} the gravitational acceleration and $\rho = 10^3$ kg m^{-3} the density of water. The angle between the direction of the wind and the positive x-direction is indicated by ϕ. For the storm network this angle is given by the SC (1926), for the tidal network these angels where determined by manually using maps found in the SC report. Although eq. (2.1) and (2.2) are different for each channel, since the depth, width, and friction coefficient are different, no channel index is present to increase the readability.

The total discharge Q ($m^3\ s^{-1}$) in a channel is given by:

$$Q = bhu \tag{2.3}$$

The time dependent wind shear stress τ_w (N m^{-2}) is represented as suggested by Pugh (1987):

$$\tau_w = C_d \rho_{air} |u_w| u_w, \tag{2.4}$$

with u_w the wind speed in $m\ s^{-1}$, $\rho_{air} = 1.225$ kg m^{-3} the density of air, and C_d the wind drag coefficient.

Boundary conditions are imposed at both ends of each channel depending on whether the ending of channel c is at open sea, at a node or at a coast:

- at open sea the water level on the North Sea is imposed (2.5),
- at a node n where several channels meet the water levels must be equal and no net flow of water can occur (2.6; 2.7),
- at the coast a no-flow condition is imposed (2.8),
- in the storm network a transport into the Zuiderzee is imposed at the entrance of the Zuiderzee (2.9).

This results in:

$$\zeta_{c,n} = \zeta_{sea} \qquad \text{for node } n \text{ at sea,} \tag{2.5}$$

$$\zeta_{1,n} = \zeta_{2,n} ... = \zeta_{q,n} \qquad \text{for } \zeta_{c,n} \text{ at node } n \text{ where } q \text{ channels meet,} \tag{2.6}$$

$$\sum_{c=1}^{q} Q_{c,n} = 0 \qquad \text{for } Q_{c,n} \text{ at node } n \text{ where } q \text{ channels meet,} \tag{2.7}$$

$$Q_{c,n} = 0 \qquad \text{for node } n \text{ at a coast,} \tag{2.8}$$

$$Q_{c.n} = Q_{out} \qquad \text{for node } n \text{ at the entrance of the Zuiderzee in the storm network.} \tag{2.9}$$

Where we use $Q_{out} = 210 \times 10^3 m^3 s^{-1}$.

2.1.3 Lorentz' linearisation of the bottom friction

The SC (1926) noted that a quadratic dependency of the bottom friction is normally used and represented the quadratic bottom friction using this parametrisation:

$$\tau_{b,quad} = \frac{g\rho}{C^2}|u|u, \tag{2.10}$$

with C the Chézy smoothness coefficient. In their tidal simulations a linear friction parametrisation was used:

$$\tau_{b,lin} = r\rho u \tag{2.11}$$

Here Lorentz linearised the bottom stress requiring that the energy dissipation over one tidal cycle is equal to that of quadratic stress. He argued that if the bottom stress were to depend linearly on velocity, he could use the superposition principle to add multiple independent water levels. This was a necessary simplification forced by computational limitations of the time. The details of his method can be found in the report of the SC (1926) and are not discussed here. He required that r should be chosen in such a way that a quadratic stress and linear stress yield the same energy dissipation over one tidal cycle, i.e.

$$r\int_{-\pi/2\omega}^{\pi/2\omega} u^2 dt = \frac{g}{C^2}\int_{-\pi/2\omega}^{\pi/2\omega} |u^3| dt,$$

with ω the angular velocity of a tidal constituent. Assuming a sinusoidal velocity signal with amplitude U_s and tidal frequency ω, by applying $u = U_s \cos \omega t$ yields:

$$r\int_{-\pi/2\omega}^{\pi/2\omega} (\cos \omega t)^2 dt = \frac{gU_s}{C^2}\int_{-\pi/2\omega}^{\pi/2\omega} |\cos \omega t|^3 dt.$$

For tides this leads to an expression for r, that is constant per channel, as shown below:

$$r = \frac{8}{3\pi}\frac{gU_s}{C^2}. \tag{2.12}$$

For storm surges — not having a tidal cycle — the energy argument cannot be applied in a straightforward manner. Therefore the linearised parametrisation that is usable for tides is not valid for storm surges. To overcome this a new linearised friction parametrisation for storm surges is used that depends on the velocity scale — and thus the cross-sectional averaged maximum flow velocity — that is constant in time. Thus this new parametrisation is also time-independent just as the tidal parametrization. The linearised friction coefficient for storm surges is written as:

$$r = \frac{gU_s}{C^2} = \frac{gU_s n^2}{h^{1/3}}, \tag{2.13}$$

with n being a Manning roughness coefficient. Here the linearised friction coefficient r is equal to the quadratic friction coefficient when the flow velocity is maximal, i.e. when $u = U_s$. The SC used a constant Chézy coefficient $C = 50\ m^{1/2}\ s^{-1}$ in their storm surge simulation. In this study a Manning coefficient $n = 0.03\ s\ m^{-1/3}$ is used corresponding to earth and winding channels according to Chow (1959).

Instead of a constant velocity scale U_s that is chosen beforehand, it would be more correct to base this velocity scale on the actual cross-sectional averaged maximum flow velocity u. For our storm model this has been done iteratively for the maximum flow velocity that occurs during a storm in every channel. A first simulation run is done with a velocity scale that is chosen before hand. After this simulation is complete the velocity scale of a channel is updated with the average of the maximum cross-sectional averaged flow velocity that occurs in that channel and the previous velocity scale (under relaxation). This is repeated until the velocity scale is equal to the actual cross-sectional averaged flow velocity.

2.1.4 Wind forcing

Only the spatially uniform time-dependent wind stress is incorporated as forcing, i.e. atmospheric pressure and wind waves are not incorporated, the spatially uniform time-dependent wind stress τ_w is represented by eq. (2.4). In their study, the SC used $\tau_w = 0.004|u_w|u_w$, following eq. (2.4) this would correspond to $C_d = 3.26 \times 10^{-3}$. In their study on the modelling the physics of storm surges Resio and Westerink (2008) noted that the drag coefficient is not greater than 2.5×10^{-3} for the region of the strongest surge generation. This wind drag coefficient is 25% lower than the one used by the SC.

Only the wind stress is made time-dependent in this study. For simplicity the direction of the wind is kept constant — as was the case in the stationary storm surge model — over all simulations and is set to 45° counter-clockwise from North, thus representing a north-westerly storm.

2.2. Solution method

The solution method is based on Chen et al. (2015; 2016). First a temporal Fourier transform is applied to the governing equations, then the differential problem is solved, and finally a superposition of the solution for each individual frequency gives the solution to the original problem in the time domain.

2.2.1 Fourier expansion

First the time-dependent wind stress is written as a superposition of time-periodic signals at different periodic frequencies using a Discrete Fourier Transformation. The continuous wind stress signal is decomposed into different signals (modes indicated by m) with different frequencies (ω_m):

$$\tau_w(t) = \sum_{m=-M}^{M} T_m \exp(i\omega_m t), \tag{2.14}$$

here T_{-m} and T_m should be complex conjugates since τ_w is real. As a result of the Discrete Fourier Transformation, a periodicity is present in the forcing, it repeats itself after a so-called recurrence period of T_{recur}, which must be chosen large enough to prevent two consecutive events from interfering as the water needs time to relax after the storm surge has passed. The frequency is given by $\omega_m = m\omega_{min}$ with $\omega_{min} = 2\pi/T_{recur}$ the lowest frequency that results from the choice of T_{recur}. T_m is the complex amplitude of the wind stress at frequency ω_m. The maximum frequency is given by $\omega_{max} = M\omega_{min}$, which determines the temporal resolution of the transformed signal.The choice of the truncation number, M, affects the amount of modes that are used in the Fourier transform. This in turn affects the quality of the representation (i.e. too few modes leads to a loss of detail) and the computational requirements (i.e. many modes leads to a higher computational load). For a wind event with a ramp up phase, constant phase, and ramp down phase the original signal (top), its amplitude spectrum (middle), and the reconstructed signal (bottom) are shown in Figure 2.3.

The expressions for the flow velocity and surface elevation in each of the channels

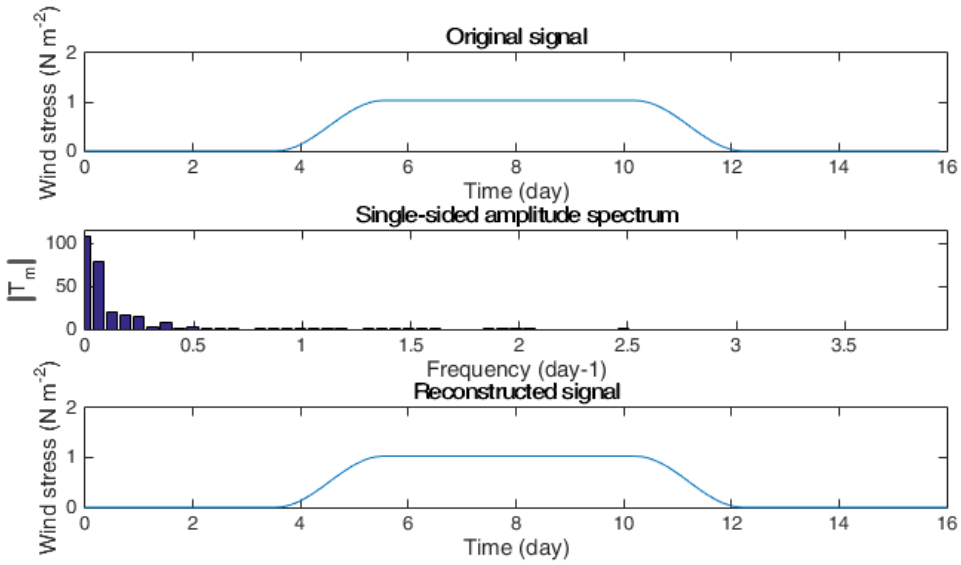

Figure 2.3: A wind stress event (top), the absolute value ($|T_m|$) single-sided amplitude spectrum obtain from the Fourier transform (middle), and the reconstructed wind stress event (bottom). Parameter values: T_{recur} = 16 days, $M = 64$.

are written similarly to eq. (2.14):

$$u(x,t) = \sum_{m=-M}^{M} U_m(x) exp(i\omega_m t), \tag{2.15}$$

$$\zeta(x,t) = \sum_{m=-M}^{M} Z_m(x)\, exp(i\omega_m t), \tag{2.16}$$

with complex velocity and elevation amplitudes $U_m(x)$ and $Z_m(x)$, respectively.

2.2.2 Boundary value problem for complex amplitudes

The above expressions are substituted into the continuity (2.1) and momentum equations (2.2), resulting in:

$$Z_m = -\frac{ih}{\omega_m} U'_m, \tag{2.17}$$

$$i\omega_m U_m + \frac{r}{h} U_m + g Z'_m = \frac{T_m}{\rho h}, \tag{2.18}$$

in which a prime indicates a derivative to x. Boundary conditions at one side of the channel ($x = 0$) read:

$$U_m(0) = U_{0,m}, \text{ and } Z_m(0) = Z_{0,m}. \tag{2.19}$$

2.2.3 Solution

By combining equations (2.17) and (2.18) an inhomogeneous Helmholtz problem is obtained for the velocity amplitude:

$$U'' + k_m^2 U = -\frac{i\omega_m T_m \cos\phi}{gh^2\rho}, \tag{2.20}$$

with mode-dependent complex wavenumber k_m:

$$k_m^2 = \frac{\omega_m^2}{gh}(1 - \frac{ir}{h\omega_m}). \tag{2.21}$$

A solution to this problem is of the form:

$$U_m(x) = A_m \exp(ik_m x) + B_m \exp(-ik_m x) - W, \tag{2.22}$$

with

$$W = \frac{i\omega_m T_m \cos\phi}{gh^2 k_m^2 \rho}, \tag{2.23}$$

in which W is a wind induced velocity and A_m and B_m are complex amplitudes. Substitution of eq. (2.22) into eq. (2.17) yields an explicit solution for Z_m:

$$Z_m(x) = -\frac{hk_m}{\omega_m}\left(A_m \exp(ik_m x) - B_m \exp(-ik_m x)\right) \tag{2.24}$$

Applying the boundary conditions (2.19) to eq. (2.22) and (2.24) yields the following expressions:

$$U_m(x) = U_{0,m}\cos k_m x - \frac{i\omega_m}{hk_m} Z_{0,m} \sin k_m x + W(\cos k_m x - 1), \tag{2.25}$$

$$Z_m(x) = Z_{0,m}\cos k_m x - \frac{ihk_m}{\omega_m} U_{0,m} \sin k_m x - \frac{ihk_m}{\omega_m} W \sin k_m x. \tag{2.26}$$

These expressions relate the flow velocity amplitude U_m and surface elevation amplitude Z_m at location x along a channel, to the flow velocity (U_0) and surface elevation (Z_0) at one end of a channel given a wind forcing. Figure 2.4 shows the water level resulting from equations (2.16) and (2.26) given only a wind forcing at the beginning of the channel, i.e. $Z_0 = 0$ and $U_0 = 0$.

2.2.4 Solution for a network

To find a solution for a network of channels we need as many equations as unknowns. Considering a network of p channels with ends either at sea or land or at an internal

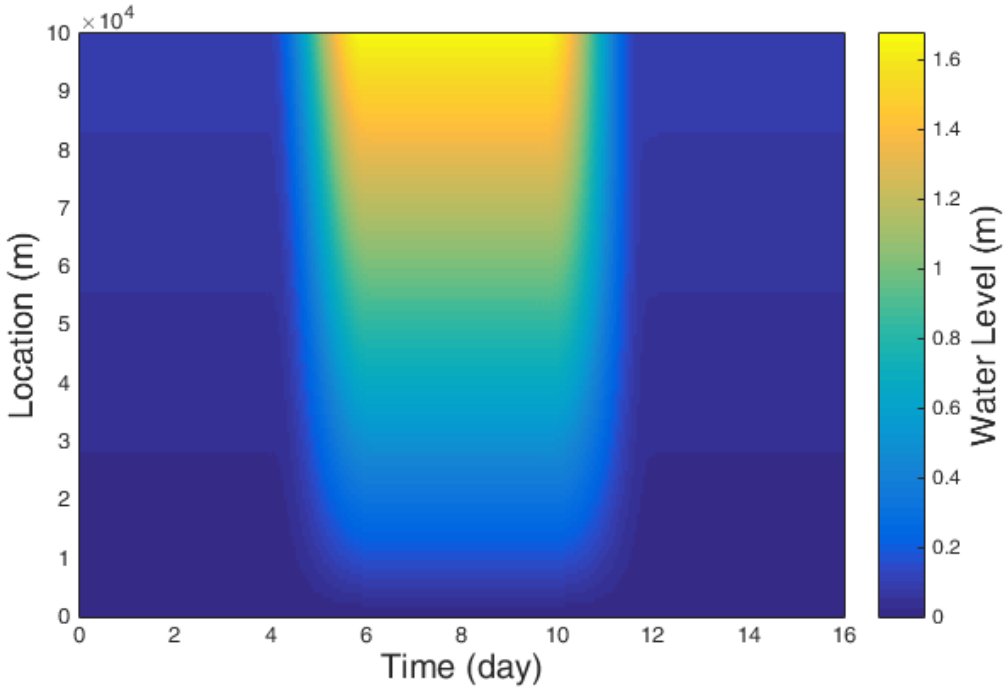

Figure 2.4: Water levels for the same wind event as in Figure 2.3 for a long channel (h=5.7m and l=100 km) resulting from equations (2.16) and (2.26)

node where multiple channels meet, the unknowns at one ending are the flow velocity u and the water level ζ. Since the two unknowns at one end are expressed in those at the other end via eq. (2.25) and (2.26), a total of $2p$ unknowns is present.

If q channels join in a node there are $q-1$ conditions that prescribe the water level must be equal in all channels at the node. Furthermore, the net flux of water at a node must vanish, so in total a node has q conditions that must be fulfilled. At every end in sea or at the coast boundary conditions are assumed, thus there are as many boundary conditions as there are channels ($2p$) and since all equations are first order, a linear system has to be solved to find the solution.

2.2.5 Relation to the SC model

Since the model described so far is based on the same governing equations and domain as the SC used, it is possible to resimulate the results that the SC found, using our model. The tidal results are obtained when (i) the wind forcing is absent (i.e. $\tau_w = 0$), (ii) oscillating water levels are prescribed as boundary conditions, and (iii) the linear friction coefficient r is written following Lorentz linearisation, see eq. (2.12). Alternatively the stationary storm surge results are obtained when the time derivatives are excluded (i.e. $\frac{\partial}{\partial t} = 0$) and a quadratic friction parametrization is used.

2.3. Simulating hydrodynamics in the Wadden Sea

The simulations and corresponding input are described in this section, upon detailing which domain representation (i.e. network), boundary conditions, wind stress, and bottom friction parametrisation are used as well as the procedure that is used to determine the velocity scale.

First the model input for reproducing the tidal results from the SC is described with an application using an iterative algorithm to determine the linear bottom friction. This is followed by the stationary simulation of the 22/23 December 1894 storm surge, simulations of non-stationary storm surges (using a time-dependent wind stress) and the sensitivity analyses.

2.3.1 Tidal simulations

The results of the SC are resimulated by using the same input as the SC, following the description of the SC (1926) and Hazewinkel (2004). The tidal results are resimulated using the tidal network (see Figure 2.1) combined with oscillating water levels representing the semidiurnal lunar tide (M_2) as seaward boundary conditions (for the

Table 2.1: Boundary conditions for channels ending at sea for both the tidal model, and the storm surge model (SC 1926, §45 and §90). The phase of the vertical tide is defined as φ in $\zeta = \hat{\zeta}\cos(\omega t - \varphi)$

Location	Vertical tide		Storm surge
	Amplitude (m)	Phase (degrees)	Water level (m)
Texel inlet	0.67	158	2.74
Eierland inlet	0.76	184	3.09
Vlie inlet	0.79	201	3.29
Borndiep inlet	0.82	225	3.47

amplitudes see Table 2.1) and a no-flow condition at the coast. Wind forcing is absent in this simulation and the bottom friction is parametrised following Lorentz' linearisation (see eq. (2.12)) with a constant velocity scale.

By using the same input used to resimulate the tidal results of the SC (i.e. tidal network, oscillating water levels and no flow boundary conditions, and no wind forcing) whilst the velocity scale is determined iteratively instead of being constant, the impact of the SC assumption of a constant velocity scale can be determined.

2.3.2 Stationary storm surge simulations

The SC reasoned that since the highest water levels occur when the measured wind speed was 16 m s^{-1}, they had to use this wind speed in their stationary storm surge simulation. The stationary storm surge results are resimulated using the storm network (see Figure 2.2), fixed water levels as seaward boundary conditions (see Table 2.1), and a constant transport ($Q_{out} = 210 \times 10^3 m^3 s^{-1}$) into the Zuiderzee as boundary condition for the node at the entrance of the Zuiderzee. The wind stress is equal to $\tau_w = 1.03$ N m^{-2} — corresponding to a wind speed of 16 m s^{-1} — using eq. (2.4) and with $C_d = 3.26 \times 10^{-3}$ following the SC. The bottom friction is parametrised following eq. (2.13) with the velocity scale being determined iteratively. Because there is a transport imposed into the Zuiderzee this simulation is not really simulating an equilibrium situation but rather a quasi-equilibrium since the Zuiderzee cannot be filled infinitely.

Next, wind event *a* consisting of a ramp up phase, a constant wind stress phase, and a ramp down phase is forced (see Figure 2.5a). This is done to verify that the same water levels are found as in the stationary storm surge simulations from the SC under the action of the same wind stress, i.e. a wind stress of $\tau_w = 1.03\,N\,m^{-2}$ is forced during

the constant wind phase. Furthermore, the storm network (see Figure 2.2) was used to represent the domain. Since this simulation is done with a time-dependent wind stress the boundary conditions are also time-dependent. The boundary conditions have a ramp up phase, a constant phase, and a ramp down phase in which they are equal to the boundary conditions in the previous simulation. Bottom friction is parametrised following eq. (2.13) with the velocity scale being determined iteratively.

2.3.3 Non-stationary storm surge simulations

Two non-stationary storm surges have been simulated. Firstly the 22/23 December 1894 storm surge to compare the timing of peak water levels and peak wind stress. Secondly, the 5 December 2013 (the 'Sinterklaas storm' or Xaver in Germany) storm surge is simulated to assess the accuracy of the model since this is a recent storm with better measurements than the 22/23 December 1894 storm. It was also an extreme storm, water levels at Harlingen exceeded 3 m + NAP, it exceeded the previous benchmark the 1 February 1953 storm for the British coast (Spencer et al., 2015), and it caused record breaking water levels on the German coast (Dangendorf et al., 2016).

First the entire duration of the 22/23 December 1894 storm is simulated. Wind event *b* is shown in the middle panel of Figure 2.5 and is derived from the SC report (1926, §26), using eq. (2.4) with $C_d = 3.26 \times 10^{-3}$, following the SC. The storm network is used, but instead of an imposed transport into the Zuiderzee, new channels have been added to represent the Zuiderzee. These channels are the same as those representing the Zuiderzee in the original tidal model with a no-flow condition at the coast. Water levels at the inlets have been derived from measurements that are given in the SC report (1926, §26). The bottom friction is parametrised following eq. (2.13) with the velocity scale being determined iteratively.

Secondly the storm of 5 December 2013 has been modelled. The wind stress at Vlieland, that is applied to the entire domain, is retrieved from the Dutch national weather service (KNMI, 2016) and is shown in the bottom panel of Figure 2.5. The wind stress formulation from eq. (2.4) has been used with $C_d = 2.5 \times 10^{-3}$. The network used for this storm is the storm network closed at the location of the Afsluitdijk. The time histories of water levels at Den Helder, Vlieland, and Wierumergronden have been retrieved from Rijkswaterstaat (2016) and are used as boundary conditions at the inlets. The bottom friction is parametrised following eq. (2.13) with the velocity scale being determined iteratively.

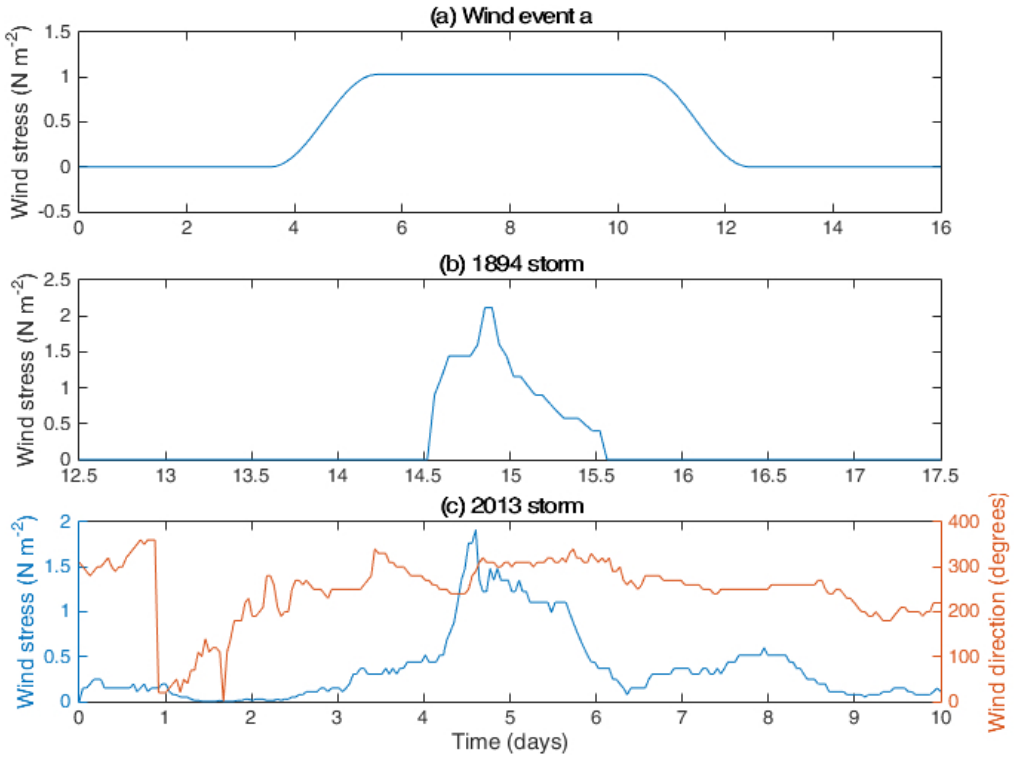

Figure 2.5: Signals of wind stresses acting in the north-westerly direction. The top panel (a) shows wind event *a* with a ramp up and ramp down period and a maximum wind stress equal to that used by the SC with T_{recur} = 16 days and M = 256. The middle panel (b) shows the wind stress for the 22/23 December 1894 storm as derived from measurements in the SC (1926) report with T_{recur} = 30 days and M = 512. The bottom panel (c) shows the wind stress for the 5 December 2013 'Sinterklaas' storm (KNMI, 2016) on the left axis and the direction for the 5 December 2013 storm on the right axis. Here 360°is North, 270°is West, 180°is South, and 90°is East. Parameter used are T_{recur} = 10 days and M = 128.

2.3.4 Sensitivity analyses

The sensitivity analyses conducted in this study provide insight in the model response to changes in:

- the roughness coefficient,
- ramp up phase duration and constant phase duration of wind event *a* (see Figure 2.5),
- domain representation,
- length of the Zuiderzee.

The roughness coefficient affects the amount of friction that the water column experiences. By comparing the maximum water levels at different locations in the Wadden Sea the effects of an increase and decrease of the bottom friction are assessed.

The ramp up phase duration and constant phase duration are two parameters that define wind event *a* (see Figure 2.5). The ramp up phase duration is the period in which the wind stress and boundary condition move from zero to their maximum value. The constant phase duration is the time while the boundary conditions and wind stress are at their maximum value. Several combinations of ramp up phase durations and constant phase durations have been used.

Since the domain is represented by a network of channels in which the water flow is constrained to only one direction, it is important to have a realistic representation of the domain. To assess this sensitivity, a denser network of channels (using the tidal network shown in Figure 2.2 including the Afsluitdijk damming the Zuiderzee) has been used. By simulating the same 2013 storm with two networks the differences in results between the two networks are assessed.

Finally, by varying the basin length — and thus the location of the Afsluitdijk — the effects of the basin length on maximum water levels in the Wadden Sea and the maximum water level at the closure dam can be assessed.

3 Results

Lorentz' tidal and storm surge results have been resimulated and new simulations have been completed, the results are presented in this chapter. Firstly the resimulated tidal results are presented. Secondly the resimulated stationary storm surge results are presented. Thirdly the results of forcing a wind event with a period of constant wind stress are presented. Fourthly the results of the non-stationary storm surge simulations are presented. Fifthly the results of the sensitivity analysis are presented.

3.1. Tidal simulations

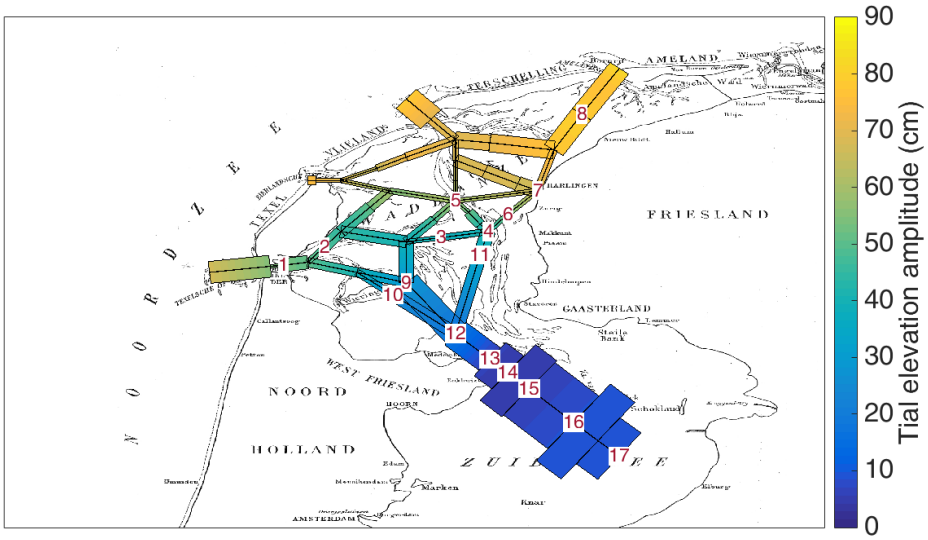

Figure 3.1: The reproduced amplitude of the vertical semidiurnal lunar tide (M_2) in the Wadden Sea, before closure. Red numbers correspond to locations in Table 3.1 and Figure 3.2.

The reproduced tidal elevation amplitude of the semidiurnal lunar tide (M_2) tide is shown in Figure 3.1. Tidal amplitudes within the Dutch Wadden Sea are lower than those offshore of the barrier islands in the North Sea, the only exception being Terschelling (top right part of the figure) where the tidal amplitude in the Wadden Sea is almost equal to the tidal amplitude in the adjacent North Sea. The lowest tidal amplitudes are found in the Zuiderzee with values below 20 cm.

For selected locations along the Dutch coast, the measurements and results of the SC

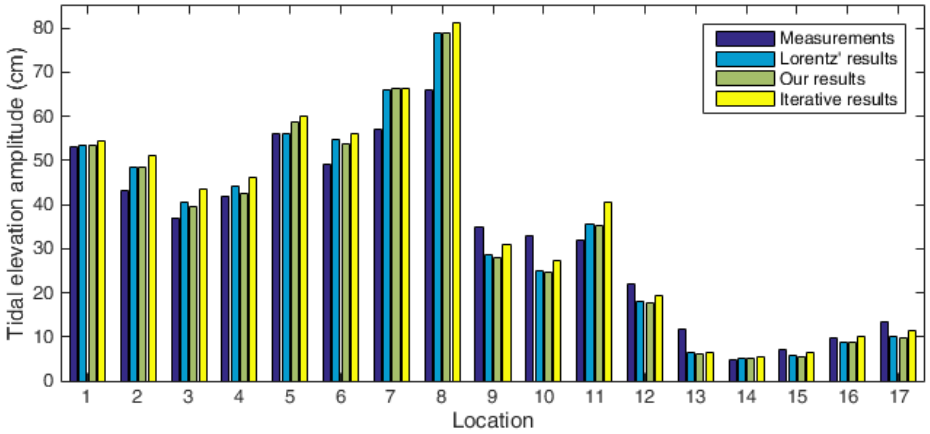

Figure 3.2: Tidal elevation amplitude (cm) of the semidiurnal lunar tide (M_2) as obtained by the SC, our model with a constant velocity scale and a velocity scale determined iteratively. Numbers indicating the location in the network correspond to those found in Figure 3.1.

are given in Table 3.1 and Figure 3.2, as well as the reproduced results with and without the iterative procedure to find the velocity scale used in the bottom friction coefficient r. Our simulation agree well with the SC results with differences within 3 cm. Differences might be caused by rounding errors or input uncertainty.

Both simulations — our tidal simulation and the tidal simulation of the SC — also agree with the measurements, although somewhat larger differences exist between them. Notable differences are found on the eastern coast of Friesland (locations 6-8), near Wieringen (locations 9 and 10), and near Enkhuizen (location 13). The SC argued that the differences on the Frisian coast and near Wieringen were caused by the exclusion of the Coriolis force, whereby a correction accounting for it led to better results. The difference between measured and observed elevation amplitude near location 8 was attributed to a measurement error, since the tide gauge fell dry during low tides resulting in a lower measured amplitude.

The results obtained using an iteratively determined velocity scale are shown in the right column of Table 3.1 and Figure 3.2. Tidal amplitudes are somewhat higher using an iterative friction coefficient, leading to a larger difference — with measurements — near the entrance of the Wadden Sea and lower differences in the Zuiderzee. Overall the differences in water levels between iterating or not iterating the velocity scale do not exceed 6 cm. This indicates that the velocity scales used by the SC yielded realistic results since there are no large differences between the results obtained using an iteratively determined velocity scale and the constant velocity scale used by the SC.

Table 3.1: Tidal elevation amplitude (cm) and phase (degrees) of the semidiurnal lunar tide (M_2) as obtained by the SC, our model with a constant velocity scale and a velocity scale determined iteratively. Numbers indicating the location in the network correspond to those found in Figure 3.1. Boxed values indicate the largest deviation from Lorentz' results.

Location	Measurements		Lorentz' model results		Rebuilt model results		Iterative model results	
	Amp.	Phase	Amp.	Phase	Amp.	Phase	Amp.	Phase
1 Den Helder	53 ± 3	168 ± 4	53.5	173	53.5	174	54.5	174
2 Oude Schild	43 ± 3	190 ± 4	48.5	187	48.3	187	51.0	187
3 Doove Balg	37 ± 3	221 ± 6	40.5	226	39.5	226	43.4	223
4 Middelgronden	42 ± 4	250 ± 6	44.2	260	42.4	263	46.1	265
5 Oude Vlie	56 ± 6	252 ± 8	56.0	253	58.7	253	59.9	254
6 Zurig	49 ± 3	253 ± 5	54.9	267	53.8	268	56.0	268
7 Harlingen	57 ± 2	260 ± 2	66.1	267	66.2	268	66.2	269
8 Nieuwe Bildt	66 ± 3	280 ± 5	79.0	267	78.9	269	81.3	270
9 Zwin	35 ± 3	225 ± 5	28.5	229	28.1	229	30.9	226
10 Westerland	33 ± 2	227 ± 3	25.0	236	24.6	236	27.3	234
11 Piaam	32 ± 4	248 ± 5	35.4	265	35.1	264	40.6	267
12 Vrouwenzand	22 ± 2	250 ± 8	18.1	255	17.7	255	19.5	252
13 Enkhuizerzand	11.8 ± 0.3	290 ± 3	6.3	291	6.1	292	6.5	292
14 Lemmer	4.7 ± 0.5	337 ± 7	5.1	329	5.0	329	5.5	331
15 Urk	7.0 ± 0.4	350 ± 4	5.8	353	5.6	353	6.5	353
16 Elburg	9.6 ± 0.6	24 ± 5	8.8	20	8.6	20	10.0	19
17 Nijkerk	13.5 ± 0.8	22 ± 4	10.0	23	9.8	23	11.3	22

3.2. Stationary storm surge simulations

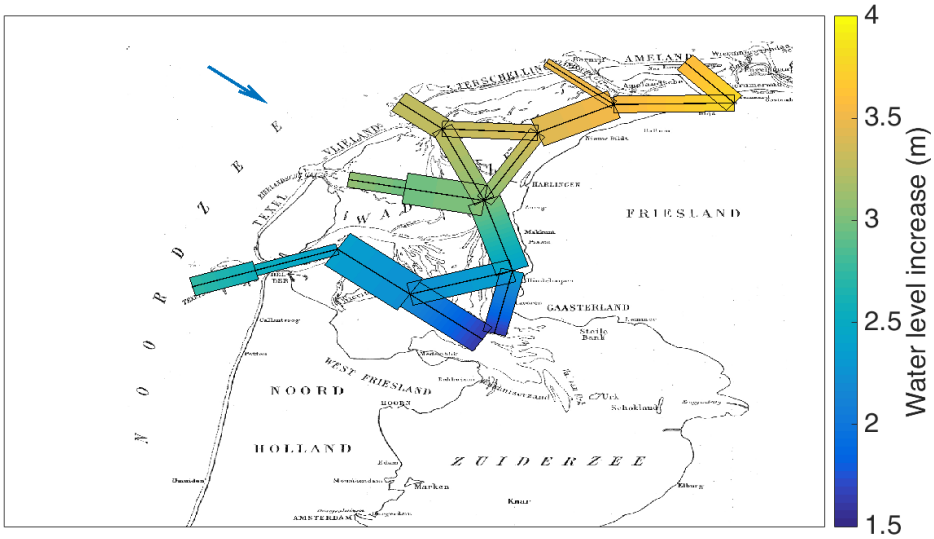

Figure 3.3: The reproduced stationary storm surge results. The blue arrow indicates wind direction.

Firstly the reproduced results are presented and secondly the results of forcing wind event *a* to mimic an equilibrium including a ramp up, constant, and ramp down phase.

The reproduced storm induced water level is shown in Figure 3.3. The storm induced water level is highest in the eastern part of the network, between Terschelling and Friesland. Here the water level increase is up to 3.5 m, whereas it is in the range 1.5 - 2 m near the entrance of the Zuiderzee.

Our model results show good qualitative agreement with those of the SC (see Figure 3.4) with differences in water levels between 1 - 15 cm. Both results indicate that the highest water levels are found between Terschelling and the Frisian coast and that the lowest water levels are found near the entrance to the Zuiderzee. The lowering of the water level near the entrance of the Zuiderzee is explained by the imposed discharge of water into the Zuiderzee, as this imposes a water level gradient down the current. Differences might be explained by a different computation method, since the original storm surge model was solved to fit the measurements, whereas in our version the velocity scale has been determined iteratively.

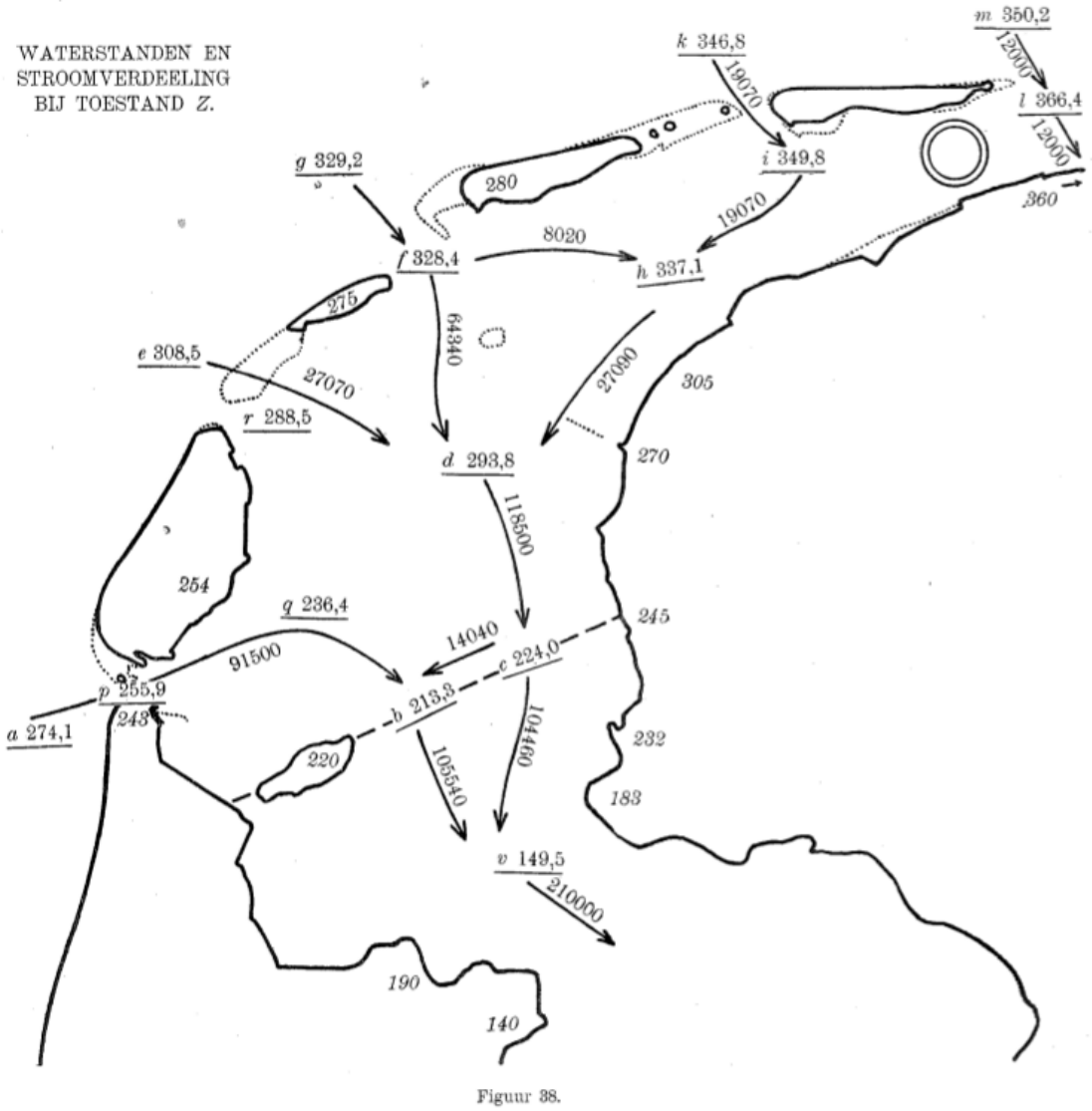

Figuur 38.

Figure 3.4: Simulated water levels in cm (underlined), measured water levels in cm (italic), and discharges in $m^3\ s^{-1}$ (next to arrows) by the SC (1926, §89).

3.2.1 Wind event *a*; constant wind stress with a ramp up and ramp down phase

The comparison between the stationary storm surge results of the SC and our non-stationary results for wind event *a* (see Figure 2.5) is shown in Figure 3.5. It shows that we obtain the almost same water levels found by the SC in their stationary storm surge simulation. The water levels increase during the ramp up phase as the wind increases and the boundary conditions increase. A decrease is found during the ramp down

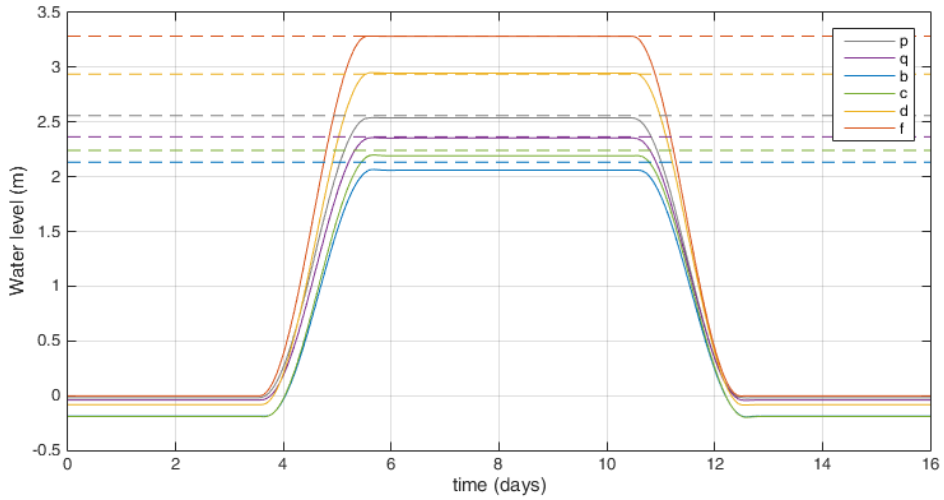

Figure 3.5: Water levels at selected point in the Wadden Sea, letters correspond to Figure 2.2, e.g. 'p' lies near Den Helder. Solid lines indicate model results, dashed lines the corresponding stationary storm results that the SC found. Here: T_{recur}= 16 days and M = 256.

phase. During the constant phase the maximum wind stress and water levels do not change and are in agreement with the water levels found in the stationary storm surge simulation.

It is also possible to determine the decay time T_{decay} at which the water adapts to changes for every channel. This has been done in Appendix B. The decay time is given by:

$$T_{decay} \sim \frac{1}{\mathrm{Im}\{\omega_m\}} = \frac{2h}{r}, \tag{3.1}$$

in which Im indicates the imaginary part of a complex number. The resulting decay times are given in Table 3.2. It shows that decay times lie between 0.6 and 5.5 hours. Since the ramp up time is much larger (48 hours) than the decay time, the change in water levels in the interior nodes corresponds to the change in boundary conditions.

Table 3.2: Decay times for channels in the storm network, channel names indicate the begin and end point of a channel.

Channel	ap	pq	qb	bv	bc	cv	dc	er	rd	fd	gf	fh	hd	ih	ki	li	ml
T_{decay} (h)	1.8	2.7	0.7	0.8	5.5	0.8	0.7	0.6	1	0.9	2.5	3.9	0.9	2.3	2.6	4.5	4.5

3.3. Non-stationary storm surges

The results of simulating non-stationary storm surges are presented in this section. First the results of the 22/23 December 1894 storm surge simulation are presented followed by the 5 December 2013 'Sinterklaas' storm simulation.

3.3.1 Simulating the 22/23 December 1894 storm

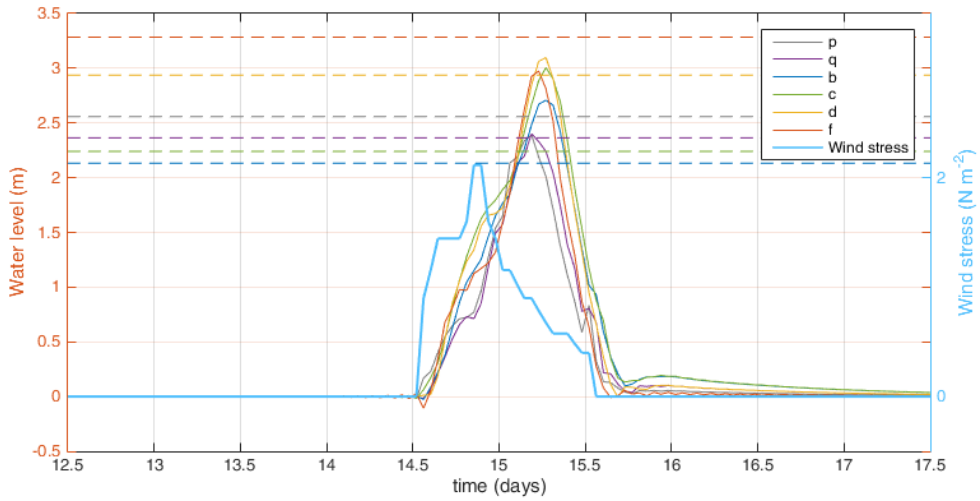

Figure 3.6: Water levels at selected point in the Wadden Sea, letters correspond to Figure 2.2, e.g. 'p' lies near Den Helder. Solid lines indicate our model results, dashed lines the corresponding stationary storm surge results obtained by the SC. The thick light blue line represents the wind stress, plotted on the right y-axis to illustrate the temporal relation between the highest water levels and highest wind stress. Here T_{recur}= 30 days and M = 512.

The 22/23 December 1894 storm has been simulated using a time-dependent wind stress and time-dependent boundary conditions at the inlets. Figure 3.6 shows that the water level peaks lags behind the wind stress. This is in accordance with the argumentation of the SC, since simulated water level peaks occur at the time that the wind stress is declining. The moment is somewhat different, as the water level peaks here occur when the wind stress is between 0.5 and 1 N m^{-2}, the SC used 1.03 N m^{-2}.

In their stationary storm surge results the SC found higher water levels near the inlets and lower water levels near the entrance of the Zuiderzee, in comparison with measurements (see Figure 3.4). The pattern of water levels found in this study agrees more with the measurements than with the stationary storm surge results (see Figure 3.4 for both). For example, near the entrance of the Zuiderzee, water levels are higher

than the SC their stationary storm surge results, although they are also higher than the measurements. Halfway in the Wadden Sea our simulated peak water levels agree with those found by the SC and their measurements. Near the inlets water levels are lower than what the SC found but they agree better with measurements.

3.3.2 Simulating the 5 December 2013 'Sinterklaas' storm

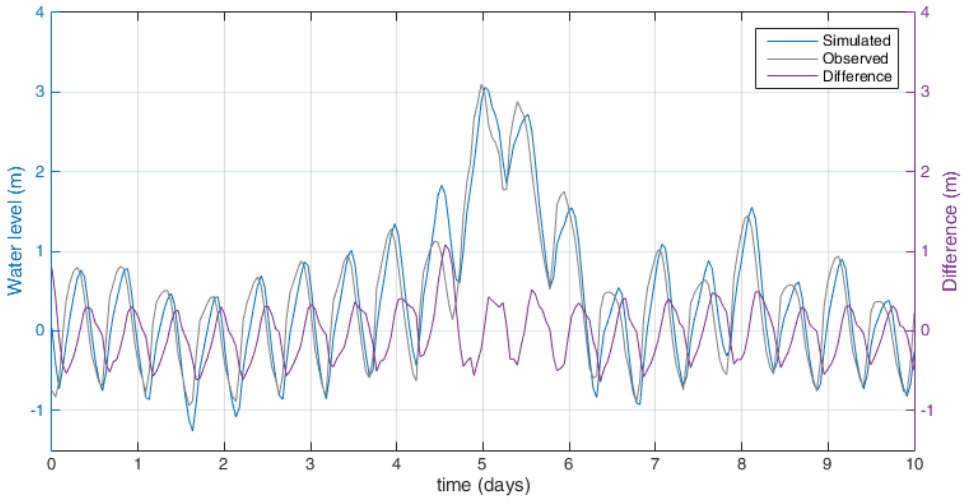

Figure 3.7: Water levels at Den Oever for the 'Sinterklaas' storm of 5 December 2013. The blue line is the simulated water level and the grey line indicates the measured water level (Rijkswaterstaat, 2016), both on the left axis. The purple line depicts the difference between the simulated and measured water levels. Here T_{recur}= 10 days and M = 128.

Next, the 5 December 2013 'Sinterklaas' storm has been simulated and the resulting water levels have been compared with measurements at three locations: Den Oever (Figure 3.7), Kornwerderzand (Figure 3.8), and Harlingen (Figure 3.9). Measurements for these locations have been obtained from Rijkswaterstaat (2016). The simulated water levels (blue lines) are in good qualitative agreement with the measurements (grey lines), both for peak timing and water levels. Significant differences (purple lines) occur at the beginning of the storm event (between day 4 and 5), when the simulated water levels are too high, especially at Kornwerderzand. Differences in simulated and observed water levels are small during the period before and after the storm, rarely exceeding a 0.1 m in difference. At the beginning of the storm differences reach up to 1 m at Kornwerderzand and up to 0.5 m at Den Oever. At Kornwerderzand a significant phase shift can be observed as the difference between simulated and observed water levels is

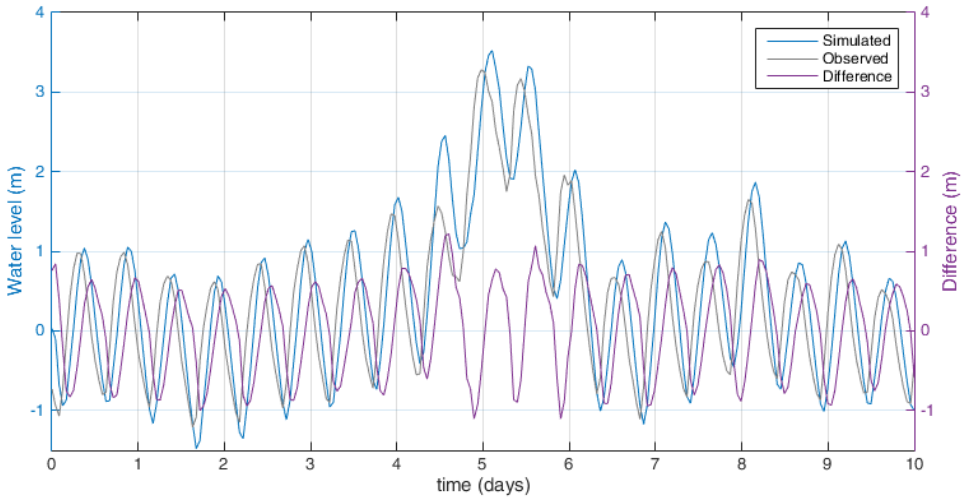

Figure 3.8: Water levels at Kornwerderzand for the 'Sinterklaas' storm of 5 December 2013. The blue line is the simulated water level and the grey line indicates the measured water level (Rijkswaterstaat, 2016), both on the left axis. The purple line depicts the difference between the simulated and measured water levels. Here T_{recur}= 10 days and M = 128.

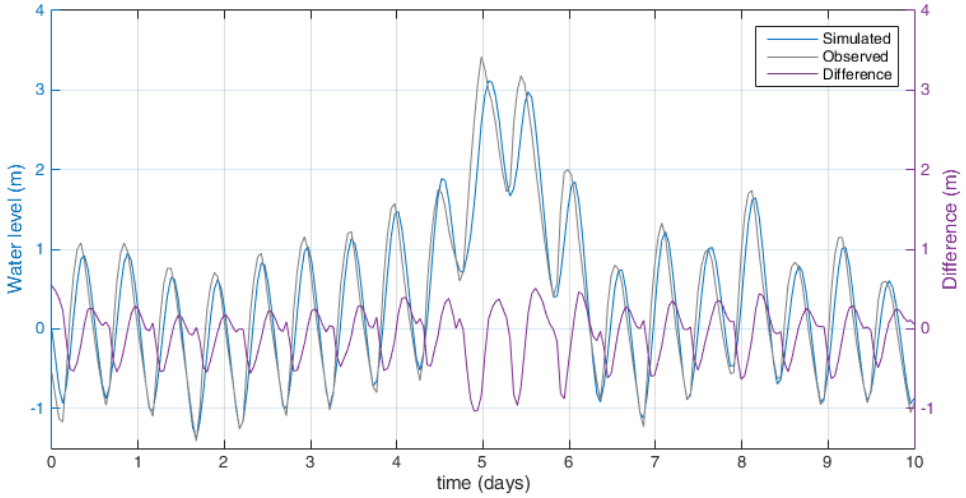

Figure 3.9: Water levels at Harlingen for the 'Sinterklaas' storm of 5 December 2013. The blue line is the simulated water level and the grey line indicates the measured water level (Rijkswaterstaat, 2016), both on the left axis. The purple line depicts the difference between the simulated and measured water levels. Here T_{recur}= 10 days and M = 128.

approaching a sine shape. The water levels at Harlingen are simulated too low for both

peaks, the difference is just under 0.5 m.

3.4. Sensitivity analyses

The results of the sensitivity analyses are presented in this section. First Manning's roughness coefficient has been varied, secondly the parameters characterizing wind event *a* (see Figure 2.5) have been varied, thirdly a different domain representation has been used to simulate the 2013 storm, and fourthly the basin length (i.e. the length of the Zuiderzee) has been varied.

3.4.1 Manning's roughness coefficient

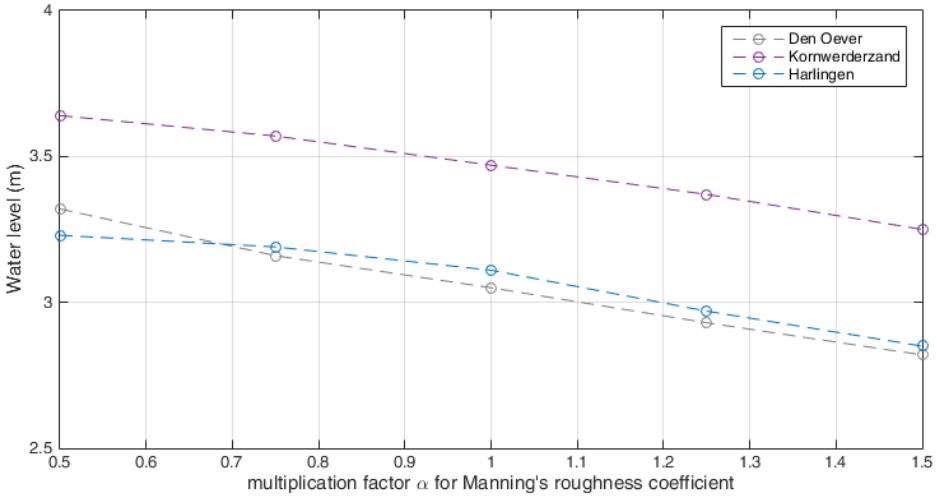

Figure 3.10: Maximum simulated water levels at Den Oever, Kornwerderzand, and Harlingen during the 'Sinterklaas' storm of 2013 for different multiplication factors for Manning's roughness coefficient. $n = \alpha n_{ref}$ with $n_{ref} = 0.03$ s $m^{-1/3}$ (eq. (2.13).

By using different values for Manning's roughness coefficient n, the friction experienced by the flow of water changes. Figure 3.10 shows that lower values of the friction coefficient (multiplication factor $\alpha < 1$) lead to higher peak water levels at the three selected locations. The opposite is true for a higher values of the friction coefficients (multiplication factor $\alpha > 1$), which result in lower peak water levels.

3.4.2 Parameters characterizing wind event *a*

The parameters characterizing wind event *a* (see Figure 2.5) have been varied and the resulting water levels at selected location are shown in Figure 3.11. It shows that, rather

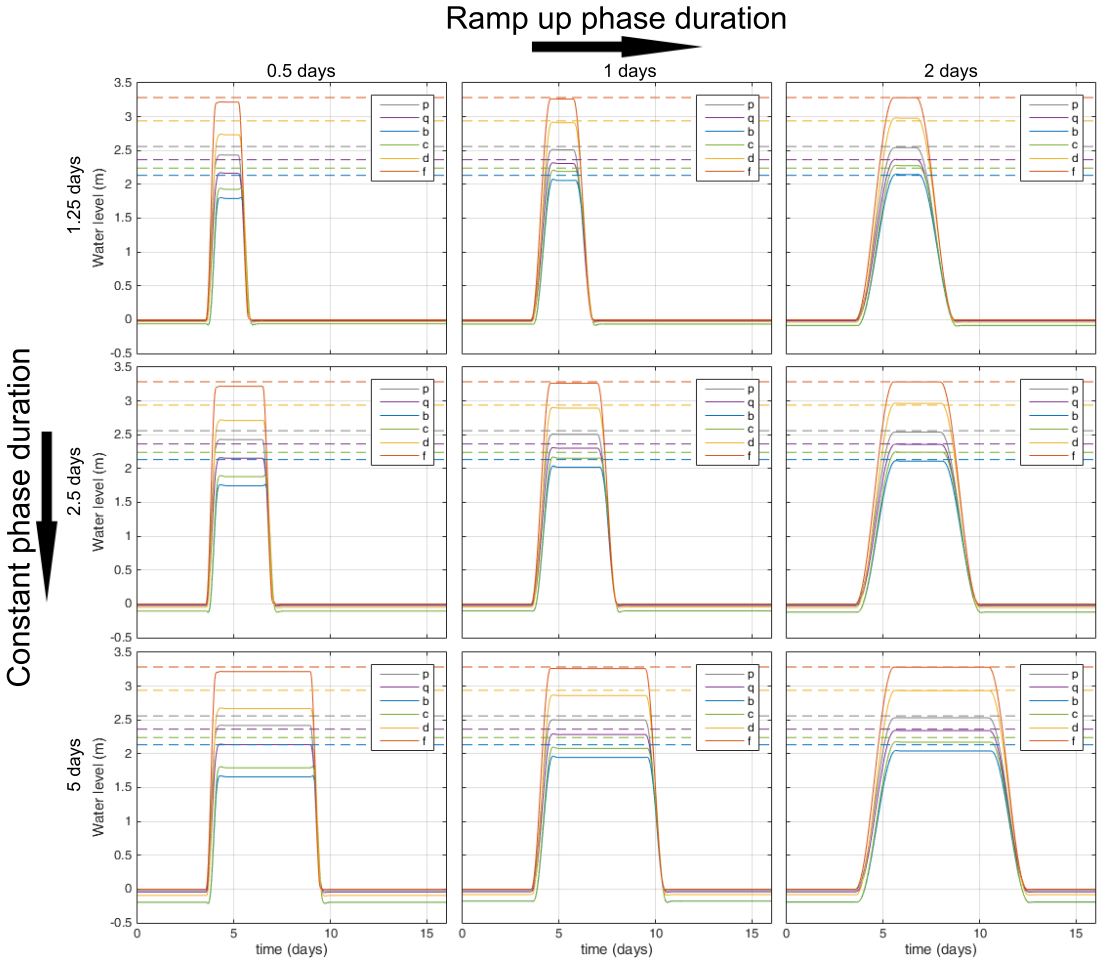

Figure 3.11: Water levels at selected locations in the Wadden Sea, letters correspond to Figure 2.2 e.g. 'p' lies near Den Helder. Different combinations of the parameters characterizing wind event *a* (see Figure 2.5) have been simulated, ramp up phase durations have been varied (0.5, 1, and 2 days) and the constant phase duration has been varied (1.25, 2.5, and 5 days). The ramp up during increases from left to right, the constant phase duration from top to bottom. Solid lines indicate model results and dashed lines the corresponding stationary storm surge water levels that the SC found. Here: $T_{recur} = 16$ and $M = 256$ for all simulations.

than the storm duration, the ramp up duration has the largest effect on the peak water levels. Discharges are also affected by the ramp up time, a shorter ramp up time results in higher peak discharges at both the beginning and the end of the storm event. This might explain the lower water levels that occur when the ramp up period is short, since a large discharge leads to a higher velocity scale and thus more bottom friction.

Since the shortest ramp up time (0.5 day = 12 hours) is comparable with the decay

time, water levels start showing relaxation behaviour when ramp up times are lower. This is observable in Figure 3.11 for short ramp up times just before the maximum water levels are reached. Therefore it is advisable to use a ramp up time that is large enough for the water level and discharge to adapt to — in this case two days.

3.4.3 Domain representation

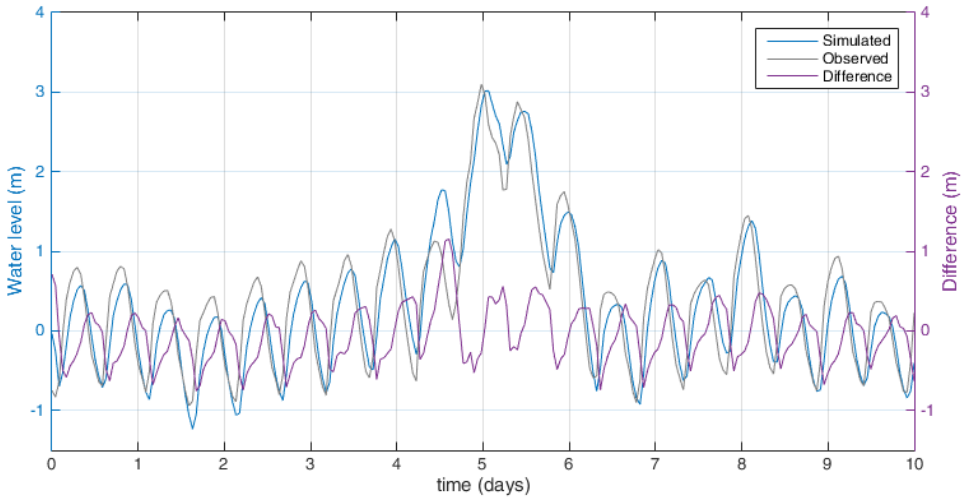

Figure 3.12: Water levels at Den Oever for the 'Sinterklaas' storm of 5 December 2013. The blue line is the simulated water level and the grey line indicates the measured water level (Rijkswaterstaat, 2016), both on the left axis. The purple line depicts the difference between the simulated and measured water levels. Here T_{recur}= 10 days and M = 128.

So far the storm network has been used in the simulations. Here the 5 December 2013 storm has been simulated using the tidal network — including the Afsluitdijk damming the Zuiderzee. Simulated and observed water level water levels are compared for Den Oever (Figure 3.12), Kornwerderzand (Figure 3.13), and Harlingen (Figure 3.14). The simulated peak timing and water levels are in relatively good qualitative agreement with the measurements. Before and after the storm the tidal water levels are underestimated, whilst during the storm water levels are overestimated. These results are lower than those obtained using the simpler storm network. Another difference is that the highest peak occurs at Harlingen instead of at Kornwerderzand. This corresponds to the measurements which show the highest water level occurred at Harlingen.

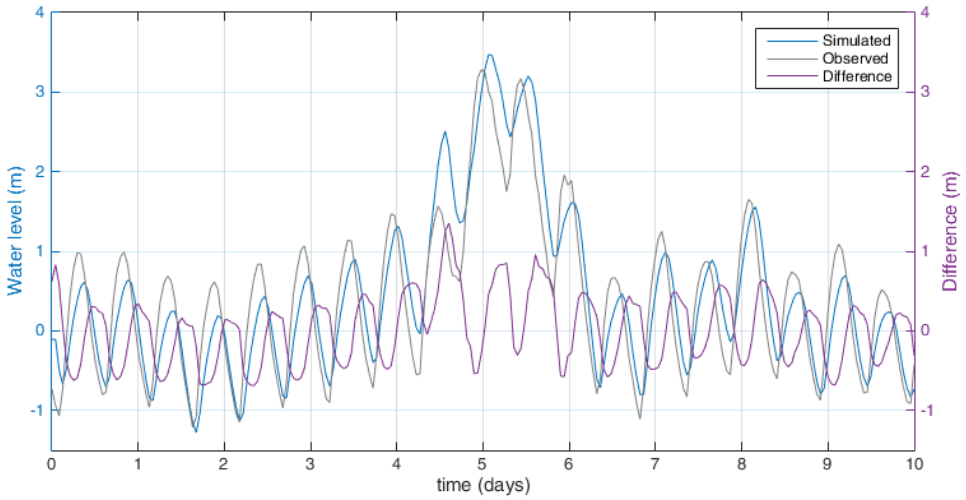

Figure 3.13: Water levels at Kornwerderzand for the 'Sinterklaas' storm of 5 December 2013. The blue line is the simulated water level and the grey line indicates the measured water level (Rijkswaterstaat, 2016), both on the left axis. The purple line depicts the difference between the simulated and measured water levels. Here T_{recur}= 10 days and M = 128.

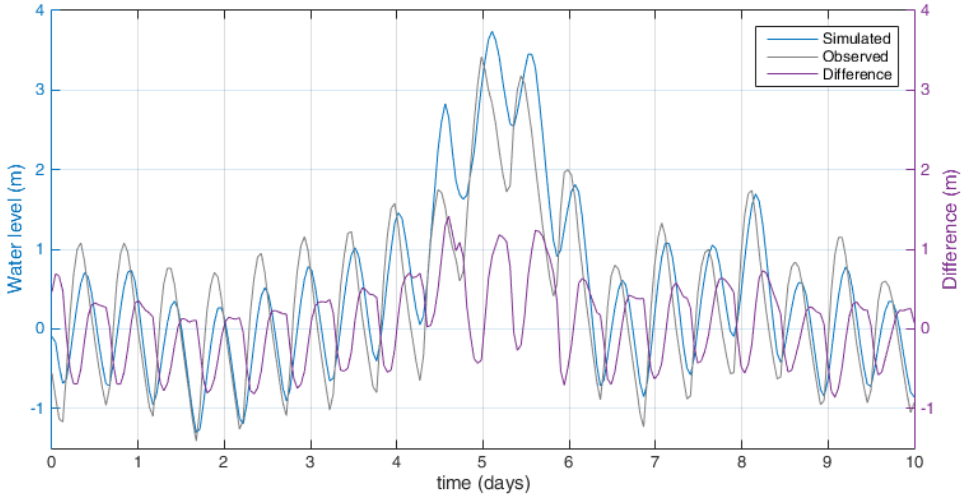

Figure 3.14: Water levels at Harlingen for the 'Sinterklaas' storm of 5 December 2013. The blue line is the simulated water level and the grey line indicates the measured water level (Rijkswaterstaat, 2016), both on the left axis. The purple line depicts the difference between the simulated and measured water levels. Here T_{recur}= 10 days and M = 128.

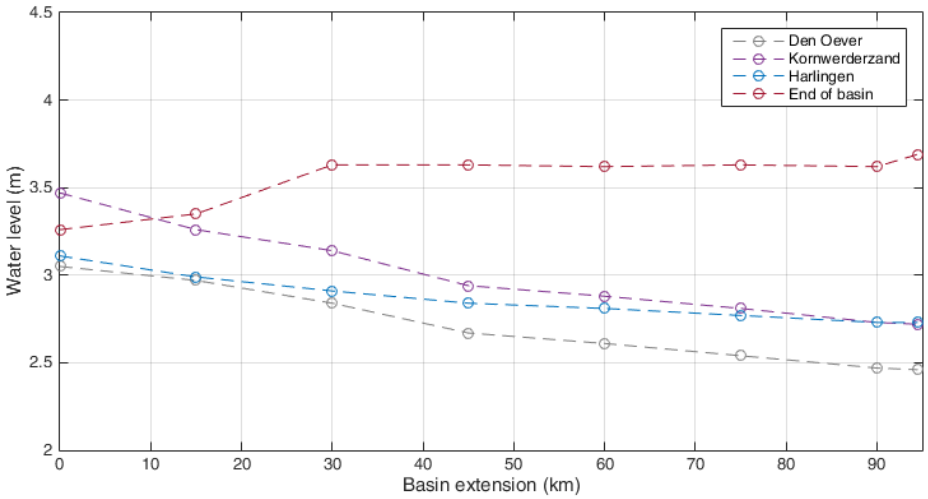

Figure 3.15: Maximum water levels at Den Oever, Kornwerderzand, Harlingen and the End of the basin simulating the 'Sinterklaas' storm of 5 December 2013 for different basin lengths. A basin extension of 0 corresponds to the present day location of the Afsluitdijk, increasing values indicate a location further south.

3.4.4 Basin length: relocating the Afsluitdijk

The Afsluitdijk dammed off the Zuiderzee from the Wadden Sea. By 'relocating' the position of the closure dam to different locations, the effect of the basin length on maximum water levels has been determined. Figure 3.15 shows the maximum water level at four locations for different basin lengths. The location 'End of basin' indicates the location of the maximum water level at the closure dam at a basin extension of 0 km the Afsluitdijk is at its current position and the maximum water level at the 'End of basin' location is the mean of that in Den Oever and Kornwerderzand. For longer basin lengths (i.e. a closure dam farther from the North Sea) 'End of basin' indicates the maximum water level at centre of the closure dam.

Figure 3.15 shows that longer basin extensions cause lower maximum water levels at Den Oever, Kornwerderzand, and Harlingen. The opposite is true for the maximum water level at the closure dam, a longer basin extension leads to higher maximum water levels at the closure dam. The change in maximum water level at the closure dam is the largest between a basin length of 0 and 30 km since the basin widens after this extension length potentially decreasing maximum water levels.

4 Discussion

In this chapter we discuss the results presented in the chapter 3. Firstly the assumptions underlying the model are discussed. Secondly, the results are interpreted, and thirdly the sensitivity of the model results is discussed.

4.1. Model assumptions

The model presented in this study is based on the linearised shallow water equations, using a time-independent linearised friction coefficient. This linearised friction coefficient, that is based on the maximum flow velocity causes an overestimation of the friction coefficient when the flow velocity is lower than the maximum flow velocity — i.e. most of the time. This is also found in the results of the 5 December 2013 storm simulation using the closed tidal network. A possible solution for this is to apply a Fourier transform to the linear friction coefficient — as has been done with the model input and output — and using linear algebra to obtain an expression for a time-dependent friction coefficient. However, this is left for future works.

It is important to consider that nonlinear dynamics play an important role in shallow basins and in tide-surge interactions. Under storm conditions the simplifications of the model are becoming less realistic, the water level elevation is no longer small in comparison to the mean water depth and linear friction is becoming less accurate with high flow velocities. This is also noted by Spencer et al. (2015) in their study on the impact of the 2013 storm on the Southern North Sea coast of the UK, according to them: "Storm surge impacts are not simply linearly related to maximum water level but rely on more complex, nonlinear interactions between tide-surge conditions". Furthermore Prandle and Wolf (1978) showed that quadratic friction is the dominant interaction mechanism between tides and storm surges on the Thames and Horsburgh and Wilson (2007) confirmed this and presented a mathematical explanation for surge clustering on the rising tide, a tidal phase shift combined with the modulation of surge production due to water depth. By including nonlinear dynamics it also becomes possible to investigate the effects of the simplifications (i.e. linear friction and assuming the water level elevation is small compared to the water depth) on the results. A possible method is given by Alebregtse and de Swart (2016) using a twofold expansion, a harmonic truncation combined with a perturbation expansion, although it should be changed so as to incorporate wind.

The channels that represent the domain only allow for a flow of water in the direction

of the channel (one dimensional flow). This means that no cross-channel flow takes place and two adjacent but not connected channels can have significantly different water levels. In their final results the SC tried to correct this by smoothing the differences between the channels (SC 1926, §92), which has not been done in this study. Strictly speaking a storm surge should be studied in two dimensions since water does flow in directions other than the channel axis, which can for instance be done with more complex models such as the Dutch Continental Shelf Model (e.g. Zijl et al., 2013). These models include more processes but also have larger computational requirements than the strongly simplified model presented in this study.

Another consideration regarding the channels is that in this entire study the channel networks from the SC have been used, thus with their configuration from the early 20^{th} century. A possibility for future works is to update the channels to the current configuration, possibly improving model results for the 5December 2013 storm, since the channel network has changed since the Afsluitdijk was built.

For simplicity the time dependent wind forcing is spatially uniform with a constant wind angle, even though these storm characteristics do influence the storm surge. In a report from Lipari and Vledder (2009) on prototype wind storms in the Wadden sea, they conclude that schematized wind storms are "not sufficient complete to reproduce historical storms" and "the peak surges for the six historical severe storms ... could not have occurred with a uniform unsteady wind". Thus a uniform wind forcing is considered insufficient to simulate peak surges and a realistic description of a storm is required. An important difference between that study and this study is that their flow model included the entire North Sea.

4.2. Interpretation of model results

A wind forcing with a ramp up phase, constant phase, and ramp down phase has been simulated and similar water levels have been found as the SC (1926,§90) found with their stationary storm surge simulation. This indicates that a temporarily equilibrium response can be obtained by forcing a constant wind stress with ramp up and ramp down phases. For shorter ramp up times the water levels do not reach the equilibrium values the SC found. This is caused by a high peak channel discharge — the result of a short ramp up durations — causing too high friction coefficients which affects the equilibrium water levels in the Wadden Sea.

The reasoning that led the SC to use a wind stress of 1.03 N m^{-2} is that the highest water levels were observed at the moment that the wind stress declined and had this value. By simulating the 1894 storm we found that the water levels reach their maximum

after the wind stress has reached its maximum. In this study it has been found that the water levels peak when the wind stress is between 1 and 0.5 N m^{-2} whereas the SC argued this was at the moment the wind stress was 1.03 N m^{-2}. An important cause for the delay in peak water level is that the water levels at the tidal inlets peak after the wind stress has peaked. Since the water enters the Wadden Sea through these inlets the water level in the Wadden Sea peak after the wind stress peak. This makes sense since calm water (i.e. not affected by a storm) in the North Sea needs to be accelerated by the wind before it reaches the Wadden Sea through the inlets. This was not covered by the stationary storm surge model that the SC used since it was time-independent.

In the stationary storm surge simulations the SC overestimated water levels near the inlets and underestimated water levels near the entrance of the Zuiderzee. The pattern of water levels found in this study agrees more with the measurements. Near the entrance of the Zuiderzee water levels are higher than both stationary results and higher than the measurements. Halfway in the Wadden Sea our simulated peak water levels agree with those found by the SC and their measurements. Near the inlets water levels are lower than what the SC found but agree better with measurements. Thus the model presented in this study performs better at simulating the 22/23 December 1894 storm surge since the results agree more with measurements, both in a qualitative and quantitative sense.

An explanation for the differences near the entrance of the Zuiderzee might also reside in the fact that the SC assumed that the influence of the Zuiderzee (i.e. the lowering of water levels in the Wadden Sea) was large during the 22/23 December 1894 storm. However Thijsse (1972) — a member of the SC and an important contributor to the SC report — remarked that this influence was small for the 22/23 December 1894 storm. From a statistical analysis of storms before and after closure, it followed that the water level at Den Oever was high in comparison to the water level at the North Sea and thus the lowering impact of the Zuiderzee was small. Assuming that a large quantity of water flows into the Zuiderzee (as the SC did) will result in an underestimation of water levels near the entrance of the Zuiderzee, as the stationary storm surge results show. Using a constant discharge into the Zuiderzee, instead of modelling it, proved to be effective since modelling the Zuiderzee would have been hard in an equilibrium model. Furthermore, one should consider the flooding of surrounding areas when water levels in the Zuiderzee become high since this increases the storage capacity of the Zuiderzee.

The model results for the 5 December 2013 storm (using the storm network) showed that the highest water levels occurred near Kornwerderzand on the Afsluitdijk. Here water levels have been overestimated. An explanation for this is that water from both

the Marsdiep inlet, near Den Helder, and the Vlie inlet, near Vlieland, flow towards Kornwerderzand before joining and reaching the end of the basin. This causes an accumulation of water resulting in higher water levels. This effect is less noticeable when the 5 December 2013 storm is simulated using the closed off tidal network, since it has a denser channel network with more interconnections between the Marsdiep inlet and Vlie inlet. This way the water is not led to Kornwerderzand from two directions, but rather spreads over the Wadden Sea. The water levels resulting form the 5 December 2013 storm simulation using the closed off tidal network are indeed lower at Kornwerderzand and higher near Harlingen. This agrees with measurements, which also indicate that the highest water levels occur near Harlingen.

The water levels during the 5 December 2013 storm are overestimated for both networks except for Harlingen in the storm network case. The highest overprediction occurs in the tidal cycle at the beginning of the storm, with overpredictions of up to 0.5 m in the storm surge network to 1 m in the closed off tidal network. An explanation for this might be that the wind stress is uniform in the domain, that is no wind energy is lost but energy is fully added to the water. The wind direction also impacts the overprediction of water levels, storms have been modelled as being entirely northwesterly whereas the 2013 storm started as a westerly storm becoming north-westerly during the storm. This might also explain why the water levels are overestimated that much at the beginning of the storm.

The tide before and after the storm is qualitatively well simulated using both networks but quantitatively the storm network performs better, as the tide is underestimated using the closed off storm network. However, the lower tidal water levels in the closed off tidal network are explained by the constant (in time and per channel) friction coefficient, that is based on the maximum flow velocities occurring during the storm event, thus resulting in high friction coefficients and lower tidal amplitudes. This effect is not observed in the storm network results, indicating that it compensates the higher friction (possibly through larger channels).

4.3. Sensitivity of model results

It has been investigated how a change in roughness coefficient affects the peak storm surge. For the 2013 storm, using the storm network, the results showed a clear trend that a lower friction coefficient leads to higher peak water levels and for higher friction coefficients lead to lower peak water levels. This makes sense since a lower friction coefficient means more water will flow into the Wadden Sea causing higher water levels and vice versa.

Additionally the effect of varying the basin length (the location of a closure dam) on peak water levels has been studied. It turns out that moving the closure dam further to the south decreases water levels at the coasts where the present-day Afsluitdijk reaches the land as well as at Harlingen. This effect is the largest for Den Oever and Kornwerderzand and smaller for Harlingen since it lies further away from the Zuiderzee. The maximum water level at the closure dam increases when the dam is moved south, the largest effect is observed between 0 and 30 km. This is explained by the geography of the basin since that is a narrow section of the Zuiderzee. After a basin extension of 30 km the water level hardly increases at the closure dam.

5 Conclusions

Using a linear model based on the model that Lorentz used to study the impact of the Afsluitdijk further insights have been obtained into the behaviour of storm surges in the Dutch Wadden Sea. The research questions formulated at the beginning of this study are answered here:

1. **How can a non-stationary model be developed based on Lorentz' approach as to simulate non-stationary storm surges forced by a time-dependent wind field?**
   A non-stationary model has been developed using a Fourier transform applied to the input (wind stress) and output (water level and flow velocity). The model is solved in the frequency domain and the superposition of the per mode solutions yield the solution to the original problem. This way the transient behaviour of storms can be studied using the model. Most simplifications that Lorentz used — linear hydrodynamics, domain representation through channels, and a constant wind direction — are reused in this model whilst the wind stress has been made time-dependent.

2. **In which aspects do the results of the non-stationary storm surge simulations differ from the results of the stationary storm surge simulation?**

   (a) **How do the results of the non-stationary storm surge simulations relate to the results of the stationary storm surge simulation?**
   The results of our model when simulating wind event *a* show that the same equilibrium water levels are found as the SC found with their stationary storm surge simulation. Thus, the new model is a suitable tool to simulate a 'temporarily equilibrium', with a spin up time and relaxation period. The new model results also show that in response to a sudden wind stress and higher water levels at the inlets the water levels in the Wadden Sea increase, first near the inlets and with a delay further in the Wadden Sea. Therefore the results of this study complement the stationary storm surge results with temporal information.

   (b) **Which insights gained from the non-stationary results cannot be found in the stationary results?**
   The non-stationary results show the spatial and temporal response to a spatially uniform unsteady wind, whereas the stationary result only show an

equilibrium response at different locations. The temporal response includes the ramp up and decay time for wind event a, and the development of water levels during a storm surge. The moment of highest water levels could be determined from the results. For the 1894 storm these moments have been compared to the moment that the wind stress peaked confirming that the water level peak is later in time than the wind stress peak, as argued by the SC.

(c) **What is the accuracy of the model if it is applied to a recent storm?**
Model runs for the 2013 storm showed that water levels are simulated qualitatively well and relatively well in a quantitative sense, with the largest overestimations just before the storm. Peak water levels during storm surges are simulated within 0.5 m of measurements, at the start of the 2013 surge water levels are overestimated, up to 1 m.

5.1. Recommendations

Based on this study the principle recommendation for further research would be to improve the model that has been developed in this study. A first improvement would be to make the linear friction coefficient time-dependent as this would results in a more accurate representation of the friction. The friction coefficient should depend on the flow velocity, which is time-dependent, whereas in this study it depends on a velocity scale that is time-independent.

A second improvement would be to make the wind direction time-dependent allowing the wind direction to change as this is what happens in reality. A third improvement would be to incorporate a spatially varying wind since the wind stress is not uniform in reality. These two improvements would improve the accuracy of the representation of the wind in the model.

A fourth improvement would be to update the channels that are used to represent the study area. The configuration used in this study dates from the early 20^{th} century and since then the bottom of the Wadden Sea has changed, something that is not reflected by the current channel configuration.

A fifth improvement would be to incorporate nonlinear dynamics since the simplifications used in this study become less realistic under storm conditions. Water level increases are no longer small compared to the mean water depth and linear friction becomes less accurate with high flow velocities. By incorporation nonlinear dynamics the it becomes possible to study the effects of these simplifications.

Bibliography

Alebregtse, N.C. and H.E. de Swart (2014). "Effect of a secondary channel on the nonlinear tidal dynamics in a semi-enclosed channel: a simple model". *Ocean Dynamics* 64 (4), pp. 573–585. DOI: 10.1007/s10236-014-0690-0.

Alebregtse, N.C. and H.E. de Swart (2016). "Effect of river discharge and geometry on tides and net water transport in an estuarine network, an idealized model applied to the Yangtze Estuary". *Continental Shelf Research* 123, pp. 29–49. DOI: 10.1016/j.csr.2016.03.028.

Alebregtse, N.C., H.E. de Swart, and H.M. Schuttelaars (2013). "Resonance characteristics of tides in branching channels". *Journal of Fluid Mechanics* 728 (10). DOI: 10.1017/jfm.2013.319.

Bakker, W.T. and H.J. de Vriend (1995). "Resonance and morphological stability of tidal basins". *Marine Geology* 126 (1-4), pp. 5–18.

Chen, W.L., P.C. Roos, H.M. Schuttelaars, M. Kumar, T.J. Zitman, and S.J.M.H. Hulscher (2016). "Response of large-scale coastal basins to wind forcing: influence of topography." *Ocean Dyn* 66 (4), pp. 549–565. DOI: 10.1007/s10236-016-0927-1.

Chen, W.L., P.C. Roos, H.M. Schuttelaars, and S.J.M.H. Hulscher (2015). "Resonance properties of a closed rotating rectangular basin subject to space- and time-dependent wind forcing." *Ocean Dynamics* 65 (3), pp. 325–339. DOI: 10.1007/s10236-015-0809-y.

Chow, V.T. (1959). *Open-channel hydraulics*. New York: McGraw- Hill Book Co. ISBN: 978-0070107762.

Dangendorf, S., A. Arns, J.G. Pinto, P. Ludwig, and J. Jensen (2016). "The exceptional influence of storm 'Xaver' on design water levels in the German Bight". *Environmental Research Letters* 11 (5). DOI: 10.1088/1748-9326/11/5/054001.

Gerritsen, H. (2005). "What happend in 1953? The Big Flood in the Netherlands in retrospect". *Philosophical Transactions of the Royal Society A: Mathematical, Physical and Engineering Sciences* 363 (1831), pp. 1271–1291. DOI: 10.1098/rsta.2005.1568.

Hazewinkel, J. (2004). *Lorentz linearization and its application in the study of the closure of the Zuiderzee*. URL: http://www.staff.science.uu.nl/~swart104/phys_coast_docs/Lorentz_zuiderzee.pdf.

Hill, A.E. and A.J. Souza (2006). "Tidal dynamics in channels: 2. Complex channel networks". *Journal of Geophysical Research* 111 (11). DOI: 10.1029/2006JC003670.

Horsburgh, K.J. and C. Wilson (2007). "Tide-surge interaction and its role in the distribution of surge residuals in the North Sea". *Journal of Geophysical Research* 112 (8). DOI: 10.1029/2006JC004033.

KNMI (2016). *Uurgegevens van het weer in Nederland*. In Dutch. URL: http://projects.knmi.nl/klimatologie/uurgegevens/selectie.cgi.

Kox, A.J. (2007). "Uit de hand gelopen onderzoek in opdracht: H.A. Lorentz' werk in de Zuiderzeecommissie". *Onderzoek in opdracht*. In Dutch. Hilversum: Verloren.

Lipari, G. and G. van Vledder (2009). *Viability study of a prototype windstorm for the Wadden Sea surges*. Alkyon. Report prepared for Deltares.

Lorentz, H.A. (1922). "Ein Rechnungsansatz für den Widerstand bei Flüssigkeitsschwindungen". *De Ingenieur* 37, p. 695.

Mazure, J.P. (1963). "Hydraulic research for the Zuiderzeeworks". Van Douwen, A.A. *In: Selected aspects of hydraulic engineering, Liber Amicorum dedicated to Johannes Theodoor Thijsse, on occasion of his retirement as professor.* TU Delft, Section Hydraulic Engineering.

Prandle, D. and J. Wolf (1978). "The interaction of surge and tide in the North Sea and River Thames". *Geophysical Journal, Royal Astrological Society* 55 (1), pp. 203–216. DOI: 10.1111/j.1365-246X.1978.tb04758.x.

Pugh, D.T. (1987). *Tides, Surges and Mean Sea-Level*. John Wiley & Sons Ltd. ISBN: 0 471 91505 X.

Resio, D.T. and J.J. Westerink (2008). "Modelling the physics of storm surges". *Physics Today* 61 (9), pp. 33–38. DOI: 10.1063/1.2982120.

Rijkswaterstaat (2016). *Waterbase*. In Dutch. URL: live.waterbase.nl.

Souza, A.J. and A.E. Hill (2006). "Tidal dynamics in channels: Single channels". *Journal of Geophysical Research* 111 (9). DOI: 10.1029/2006JC003469.

Spencer, T., S.M. Brooks, B.R. Evans, J.A. Tempers, and I. Möller (2015). "Southern North Sea storm surge event of 5 December 2013: Water levels, waves and coastal impacts". *Earth-Science Reviews* 146, pp. 120–145. DOI: 10.1016/j.earscirev.2015.04.002.

State Committee on the Zuiderzee (1926). *Report of the State Committee on the Zuiderzee*. report. In Dutch. 's-Gravenhage: Algemene Landsdrukkerij.

Stelling, G.S. (1983). "On the construction of computational methods for shallow water flow problems". Dissertation. TU Delft.

Stroband, H.J. and N.J. Wijngaarde (1977). "Modelling of the Oosterschelde estuary by a hydraulic model and a mathematical model". *Proceeding for the: Seventeenth Congress of the International Association for Hydraulic Research, Baden-Baden, August 15-19,1977*.

Thijsse, J. Th. (1972). *Een halve eeuw Zuiderzeewerken*. In Dutch. Groningen: H.D. Tjeenk Willink B.V.

United States Geological Survey, USGS (2016). *LandsatLook Viewer: a prototype tool that allows rapid online viewing and access to the USGS Landsat archive*. URL: `http://landsatlook.usgs.gov`.

Zijl, F., M. Verlaan, and H. Gerritsen (2013). "Improved water-level forecasting for the Northwest European Shelf and North Sea through direct modelling of tide, surge and non-linear interaction". *Ocean Dynamics* 63 (7), pp. 823–847. DOI: `10.1007/s10236-013-0624-2`.

Appendices

A Channel data

TABEL 19.

Ligging.	Lengte. km	Dwarsprofiel. Hoofdgeul. $b_1 \times q_1$	$b_2 \times q_2$	$b_3 \times q_3$	Hoek wind-as geul (ongeveer).
Haaksgronden . . . . . *a p*	10	8,0 × 9,0	2,0 × 20,0	—	70°
Binnenkant Heldersche zeegat . . *p q*	13	2,0 × 27,0	2,0 × 15,0	2,0 × 8,0	70°
Binnenkant Texelstroom . . . . *q b*	15	20,5 × 4,0	1,5 × 20,0	1,0 × 10,0	0°
Wieringer Vlaak . . . . . *b v*	15	17,5 × 6,25	—	—	0°
Breezand . . . . . *b c*	16	12,0 × 6,0	—	—	65°
Friesche Vlaak . . . . . *c v*	15	14,8 × 7,0	—	—	55°
Zuidoostrak . . . . . *d c*	17	9,0 × 6,0	1,5 × 16,0	10,5 × 4,0	30°
Eierlandsche zeegat . . . . . *e r*	8,5	1,5 × 10,0	2,5 × 6,0	4,0 × 1,0	30°
Waardgronden . . . . . *r d*	12	14,0 × 3,5	2,0 × 8,0	—	30°
Inschot-Vliestroom . . . . . *f d*	19	1,3 × 18,0	9,7 × 4,0	2,0 × 9,0	20°
Buitengronden Vlie . . . . . *g f*	9	11,0 × 9,0	2,0 × 18,0	—	0°
Meepen. . . . . *f h*	14	1,0 × 16,0	2,0 × 9,0	5,0 × 4,0	40°
Vlakte van Oosterbierum . . . . *h d*	16	4,0 × 6,5	6,0 × 3,5	—	90°
Terschellinger Wad. . . . . *i h*	13	16,0 × 5,0	—	—	105°
Amelandsche zeegat. . . . . *k i*	14	1,2 × 21,0	3,8 × 5,0	—	0°
Amelandsche Wad . . . . . *l i*	19	8,5 × 5,5	—	—	120°
Zeegat van Schiermonnikoog. . . *m l*	13	11,0 × 5,0	1,5 × 12,0	—	0°

b in km; *q* in meters.

Figure A.1: Channel data for the storm network. Table 19 from the SC report (1926, §89). B is the channel width in km and q the mean water depth in m.

TABEL 6. **Geulennet van berekening Za.**

Geul.		O	l	Dwarsprofiel.				v_m	S	C^2
N°.	Ligging.			$b_1 \times q_1$	$b_2 \times q_2$	$b_3 \times q_3$	$b_4 \times q_4$			
1*a*	Haaks	113	10,0	2500 × 16	8800 × 4	—	—	80 [1]	54,88	280000
1*b*	Helsdeur	4	2,2	1200 × 35	600 × 15	—	—	125	61,16	Bazin
1*c*	Marsdiep	29	4,2	2600 × 20	1200 × 10	3100 × 0	—	110	67,17	id.
2	Malzwin	48	9,5	1100 × 12	1200 × 2	2700 × 0	—	100	14,07	id.
3*a*	Texelstroom West	18	5,2	1700 × 25	700 × 9	1050 × 0	—	105	49,16	id.
3*b*	Texelstroom Midden	35	5,0	1900 × 18	1000 × 10	4100 × 0	—	100	42,09	id.
4*a*	Doove Balg West	15	6,3	550 × 15	1900 × 2,5	—	—	75	7,85	280000
4*b*	Doove Balg Oost	30	9,0	300 × 11	1600 × 2,5	1400 × 0	—	90	4,57	Bazin
5*a*	Scheurrak	49	9,2	400 × 11	4900 × 0	—	—	90	3,96	280000
5*b*	Oude Vlie	31	7,5	250 × 9	3900 × 0	—	—	75	1,69	Bazin
6*a*	Middelgronden Noord	17	3,2	1000 × 11	2500 × 4	1800 × 0	—	90	5,58	280000
6*b*	Zuidoostrak Zuid	33	5,2	700 × 11	500 × 3	5200 × 0	—	75	6,41	id.
6*c*	Zuidoostrak Noord	14	5,1	900 × 10	1900 × 0	—	—	85	7,65	id.
7*a*	Boontjes Zuid	15	4,8	700 × 7	1500 × 1	1000 × 0	—	85	4,66	id.
7*b*	Boontjes Noord	22	6,8	3200 × 2,5	—	—	—	40	3,20	id.
8*a*	Inschot Zuid	14	5,0	900 × 11	1900 × 0	—	—	85	8,42	id.
8*b*	Inschot Noord	13	5,0	700 × 13	1900 × 0	—	—	95	8,64	id.
9*a*	Pollen	32	4,0	3000 × 3	5000 × 0	—	—	40	3,60	id.
9*b*	Zuidrak	47	6,5	700 × 6	2600 × 3	4000 × 0	—	80	7,84	id.
9*c*	Blauwe Slenk	40	5,8	900 × 11	6000 × 0	—	—	110	10,89	Bazin
10	Vlakte v. Oosterbierum	53	11,5	3000 × 2,5	1600 × 0	—	—	40	3,00	280000
11	Vliestroom	13	3,8	1200 × 17	2100 × 0	—	—	115	23,46	id.
12*a*	Oostmeep	112	12,0	800 × 13	1800 × 7	6700 × 0	—	90	18,06	id.
12*b*	Meep	52	6,4	1000 × 16	700 × 10	6500 × 0	—	115	24,98	id.
13*a*	Boomkensdiep	33	6,0	1800 × 20	3700 × 6,5	—	—	110	55,70	Bazin
13*b*	TerschellingerGronden	97	6,0	1400 × 13	6000 × 6	8800 × 3	—	110	62,50	280000
14	Vlieter	85	9,0	2300 × 7	3000 × 4,5	2100 × 2,5	2000 × 0	65	19,31	Bazin
15*a*	Friesche Vlaak	174	20,5	8500 × 4	—	—	—	30	10,20	280000
15*b*	Middelgronden Zuid	54	6,0	500 × 8	3000 × 5	4300 × 2	1200 × 0	70	13,75	Bazin
16*a*	Knar	365	10,0	36500 × 2,5	—	—	—	5,5	5,02	id.
16*b*	Marken-Elburg	738	12,0	61500 × 3,5	—	—	—	7	15,07	id.
16*c*	Elburg-Urk	935	22,0	42500 × 4	—	—	—	13	22,10	id.
16*d*	Val van Urk	455	10,0	45500 × 4,5	—	—	—	18	36,80	id.
16*e*	Enkhuizerzand	238	9,0	26500 × 5	—	—	—	24,5	32,46	id.
16*f*	Nauw van Stavoren	297	16,5	8000 × 7	10000 × 3	—	—	43	32,46	id.
17	Wieringer Vlaak	261	16,5	2500 × 6	13300 × 3,6	—	—	45	23,25	id.
18	Wierbalg	49	9,7	700 × 6,5	900 × 3,5	3500 × 0	—	75	5,18	280000
19*a*	Amsteldiep	45	11,3	500 × 8	700 × 5	2800 × 0	—	80	5,38	Bazin
19*b*	Wieringer Meer	138	19,5	5100 × 3	2000 × 2	—	—	25	4,66	280000
20*a*	Abt	105	8,0	1000 × 5	4000 × 2	8200 × 0	—	75	7,59	id.
20*b*	Kromme Balg	134	22,0	Dwarsprofiel ongeveer 13000 m².				—	12	id.
22	Molenrak	30	12,5	2400 × 2,5	—	—	—	30	1,80	id.
23	Texelstroom Oost	57	9,2	2000 × 18	1000 × 3,5	3200 × 0	—	90	33,98	id.
24*a*	Binnenbreesem	60	8,5	1600 × 2,5	1500 × 1	4000 × 0	—	50	2,48	id.
24*b*	Foksdiep	32	5,5	400 × 5	1000 × 1	4500 × 0	—	70	1,72	id.
25	Driesprongplaat	36	12,0	200 × 4	1000 × 1	1800 × 0	—	80	1,04	id.
26	Vogelzwin	23	10,3	600 × 8	600 × 1,5	1000 × 0	—	100	5,20	id.
27*a*	Kolk	14	6,8	700 × 4,5	1400 × 0	—	—	80	2,52	id.
27*b*	Vianensveldje	23	5,8	500 × 4	3400 × 0	—	—	75	1,50	id.
27*c*	Vliesloot	44	9,5	1200 × 4	3400 × 0	—	—	75	3,60	id.
28*a*	Eierlandsche Gat	8	3,7	300 × 14	400 × 6	1500 × 3	—	110	8,54	id.
28*b*	Stanley	6	1,3	1600 × 4,5	3100 × 2	—	—	85	9,65	id.

Figure A.2: Channel data for the tidal network. Table 6 from the SC report (1926, §45). O is the surface area of the channel in km^2, l the length in km, B the width in m, q the mean water depth in m, v_m the velocity scale in $cm\ s^{-1}$, S the corresponding discharge in $1000 m^3\ s^{-1}$, and C^2 the square of the Chézy coefficient in $cm\ s^2$.

B Decay time

The decay time that is presented in this study has been determined using the equations governing the hydrodynamics presented in chapter 2. From equations:

$$\frac{\partial \zeta}{\partial t} + h\frac{\partial u}{\partial x} = 0, \tag{B.1}$$

$$\frac{\partial u}{\partial t} + \frac{r}{h}u = -g\frac{\partial \zeta}{\partial x}, \tag{B.2}$$

one can obtain:

$$\frac{\partial^2 \zeta}{\partial t^2} - \frac{r}{h}\frac{\partial \zeta}{\partial t} - gh\frac{\partial^2 \zeta}{\partial x^2}. \tag{B.3}$$

A solution to eq. (B.3) is written similarly as eq. (2.16):

$$\zeta(x,t) = \sum_{m=-M}^{M} Z_m(x)\exp(i\omega_m t). \tag{B.4}$$

Assuming that the elevation amplitude behave sinusoidal, an expression for every mode is found:

$$\zeta_m(x,t) = \exp(i\omega_m t)\cos(\frac{m\pi x}{l}). \tag{B.5}$$

By combining equations (B.3) and (B.5) an expression for ω_m can be found:

$$\omega_m = \frac{ir}{2h} \pm \sqrt{gh(\frac{m\pi}{l})^2 - (\frac{r}{2h})^2}. \tag{B.6}$$

Thus the decay time, being similar to $\frac{1}{Im(\omega_m)}$, is given by:

$$T_{decay} \sim \frac{1}{Im(\omega_m)} = \frac{2h}{r}. \tag{B.7}$$

The decay time is given by eq. B.7 if the square root in eq. (B.6) does not produce imaginary numbers, i.e. $gh(\frac{m\pi}{l})^2 > (\frac{r}{2h})^2$.